# A Medium Power Traveling-Wave Tube for 6,000-Mc Radio Relay

By J. P. LAICO, H. L. McDOWELL and C. R. MOSTER

(Manuscript received May 15, 1956)

*This paper discusses a traveling-wave amplifier which gives 30 db of gain at 5 watts output in the 5,925- to 6,425-mc common carrier band. A description of the tube and detailed performance data are given.*

## TABLE OF CONTENTS

## I. INTRODUCTION

During the past ten years traveling-wave tubes have received considerable attention in vacuum tube laboratories, both in this country and abroad. So far their use in operating systems has been somewhat limited, the most notable exceptions being in radio relay service in France, Great Britain, and Japan. However, it appears that sufficient progress in both tube and system design has been made so that traveling-wave tubes may see widespread application in the near future.

This paper describes an experimental helix type traveling-wave tube representative of a class which may see extensive use as a power amplifier in radio relay systems. The tube is designated as the Bell Laboratories type MI789. Stated briefly, the performance characteristics under nominal operating conditions are:

Frequency Range........................5,925–6,425 mc
Power Output.................................5 watts
Gain at 5 watts output.........................31–35 db
Noise Figure.................................< 30 db

The tube is designed for use with waveguide input and output circuits. The input voltage standing wave ratio (VSWR) is less than 1.1 and the output VSWR is less than 1.4 over the 500-mc band when the tube is delivering 5 watts of output. Fig. 1 shows a photograph of an MI789 and of an experimental permanent-magnet focusing circuit.

In developing this tube we have endeavored to produce an amplifier which could be considered "practical" for use in a transcontinental radio relay system. Because such an application requires a high degree of reliability and refinement in performance, the tube was rather conservatively designed. This made it possible to obtain the desired gain and power output without difficulty. On the other hand, the contem-
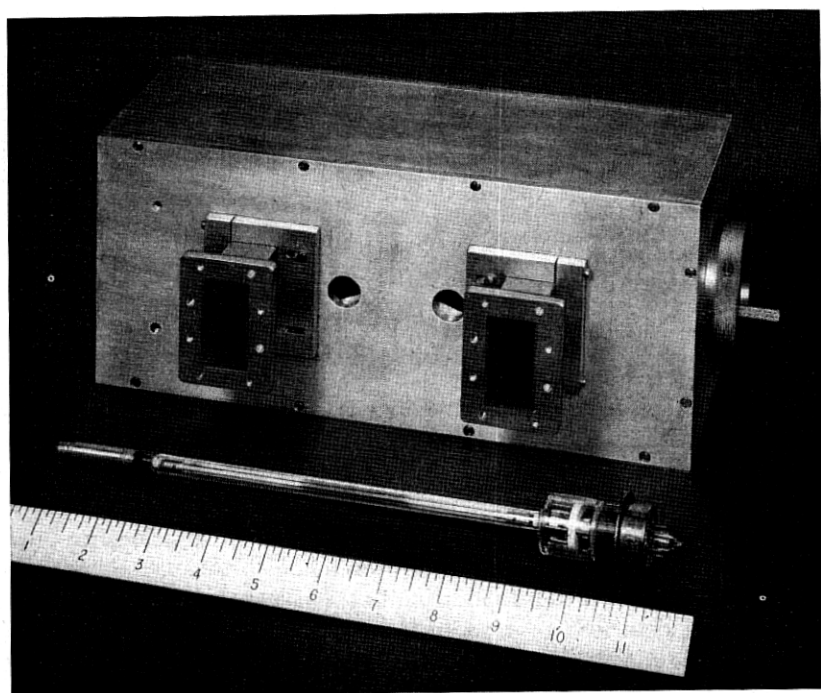


Fig. 1 — The MI789 traveling-wave tube and an experimental permanent magnetic circuit used to focus it. The circuit contains two specially shaped bar magnets between which the tube is mounted. The magnetic flux density obtained is 600 gauss, and the overall circuit weight is about 25 pounds.

plated system application made it necessary to investigate in detail the problems associated with band flatness, matching, noise output, certain signal distortions, reproducibility, and long life.

The solution of some of these problems required the development of a precisely constructed helix assembly in which the helix winding is bonded to ceramic support rods by glaze. Others required the initiation of a life test program. Early results indicate that life exceeding 10,000 hours can be obtained. This, in no small measure, is a result of a dc potential profile which minimizes the ion bombardment of the cathode. Since power consumed by focusing solenoids seriously degrades the overall efficiency of a traveling-wave amplifier, permanent magnet focusing circuits such as the one shown in Fig. 1 have been designed. Finally, to further improve efficiency, a collector which can be operated at about half the helix voltage was developed.

The major difficulties encountered in the course of the MI789 development were: excessive noise output, ripples in the gain-frequency characteristic, and lack of reproducibility of gain. There is evidence that a growing noise current wave on the electron stream was the source of the high noise output. This phenomenon has been observed by a number of experimenters but is not yet fully explained. By allowing a small amount of the magnetic focusing flux to link the cathode, the growing noise wave was eliminated, and the noise reduced to a reasonable level for a power amplifier. Reflections caused by slight non-uniformities in the helix pitch were the source of the gain ripples. Precise helix winding techniques reduced these reflections so that the ripples are now less than ±0.1 db. The lack of reproducibility in gain was caused by variations in helix attenuation. Here, too, careful construction techniques alleviated the problem so that in a recent group of tubes the range of gain variation at five watts output was ±2 db.

We have divided this paper into four main parts. The next section discusses some of the factors affecting the design of the traveling-wave tube. (We will henceforth use the abbreviation TWT.) Section III describes the tube itself. Certain performance data are included there when closely related to a particular portion of the tube. Section IV considers the rf performance in detail. There comparisons are made between the performance predicted from TWT theory and that actually observed. Finally Section V summarizes our life test experience.

This paper is written primarily for workers in the vacuum tube field and assumes knowledge of TWT theory. However, we believe that readers interested in TWT's from an application standpoint may also benefit from the discussion of the rf performance in Section IV. Much of that section can be understood without detailed knowledge of TWT's.

## II. DESIGN CONSIDERATIONS

While TWT theory served as a general guide in the development of the MI789, a number of important tube parameters had to be determined either by experimentation or by judgement based on past experience. The most important of these were:

Saturation power output........................12 watts
Mean helix diameter............................90 mils
$\gamma a$.........................................$\sim$ 1.6
Magnetic flux density...........................600 gauss
Cathode current density.....................$\sim$ 200 ma/cm$^2$

These quantities and the requirement of 30-db gain at five watts output largely determined the TWT design.

The saturation output of 12 watts was found necessary to obtain the desired linearity at five watts output and the $\gamma a$ value of 1.6 to obtain the flattest frequency response over the desired band.

The choice of helix diameter and magnetic flux density represented a compromise. For the highest gain per unit length, best efficiency, and lowest operating voltage, a small helix diameter was called for. On the other hand, a large helix diameter was desirable in order to ease the problem of beam focusing and to facilitate the design of a light-weight permanent magnet focusing circuit. In particular, the design of such a circuit can be greatly simplified if the field strength required is less than the coercive force of available magnetic materials. This allows the use of straight bar magnets instead of much heavier horseshoe magnets. Moreover, the size and weight of the magnetic circuit is minimized by employing a high energy product material. These considerations led us to choose a flux density of 600 gauss, thereby permitting us to design a magnetic circuit using Alnico bar magnets.

To obtain long tube life we felt it desirable to limit the helix interception to about one per cent of the beam current. On the basis of past results we estimated that this could be done with a magnetic flux density 2.6 times the Brillouin value for a beam entirely filling the helix. With this restriction, Fig. 2 shows how the TWT design is affected by varying the helix diameter. A choice of 600 gauss is seen to result in a mean helix diameter of 90 mils.

In the selection of cathode current density, a compromise between long life and ease of focusing had to be made. To obtain long life, the current density should be minimized. However, this calls for a highly convergent gun which in turn complicates the focusing problem. We decided to use a sprayed oxide cathode operating at about 200 ma/cm$^2$. Experience with the Western Electric 416B microwave triode had shown
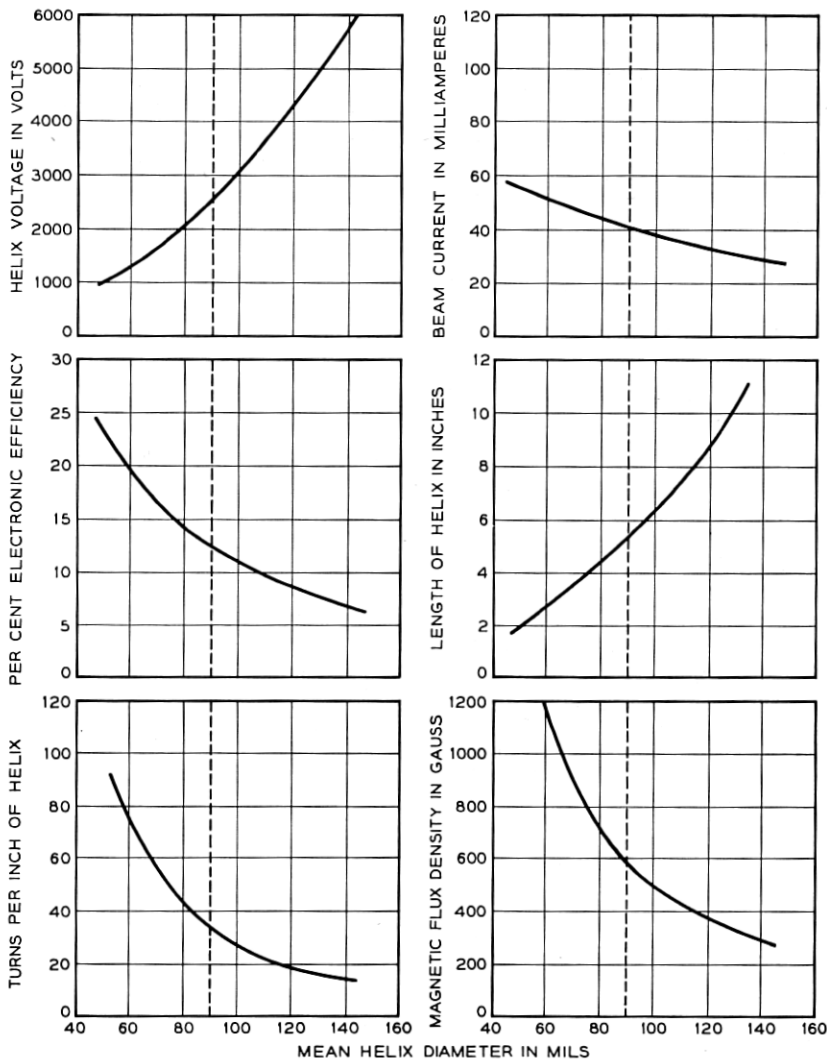
Fig. 2 — Alternate designs for the M1789. These curves are an estimate of how the TWT design would be affected by changing the helix diameter. They represent essentially a scaling of the M1789 design. In all cases the expected maximum power output is 12 watts and the low-level gain is 33 db. The line at 90 mils mean diameter in the curves represents the present M1789 design. In these calculations it was assumed that:

   a. $\gamma a = 1.6$
   b. power output $= 2.1\ CI_0V_0 = 12$ watts
   c. the magnetic flux density is 2.6 times the Brillouin flux density for a beam entirely filling the helix.
   d. the ratio of wire diameter to pitch is 0.34.
   e. the dielectric loading factor is 0.79.
   f. the ratio of effective beam diameter to mean helix diameter is 0.5.

1289

## TABLE I — SUMMARY OF M1789 DESIGN

I. Helix Dimensions

| | | |
|---|---|---|
| Mean Diameter | 90 | mils |
| Inside Diameter | 80 | mils |
| Wire Diameter | 10 | mils |
| Turns per Inch | 34 | |
| Pitch | 29.4 | mils |
| Wire Diameter/Pitch | 0.34 | |
| Active Length | $5\frac{1}{2}$ | inches |

II. Voltages and Currents

| Electrode | Voltage (volts) | Current (ma) |
|---|---|---|
| Cathode | 0 | 40 |
| Beam Forming Electrode | 0 | 0 |
| Accelerator | 2600 | < 0.1 |
| Helix | 2400 | <0.4 |
| Collector | 1200 | >39.5 |
| Heater Power | 6 watts | |

III. TWT Parameters at Midband (6175 mc)

| | |
|---|---|
| $\gamma a$ | 1.58 |
| $ka$ | 0.148 |
| $C$ | 0.058 |
| $QC$ | 0.29 |
| $N$ (number of $\lambda$'s on helix) | 30 |
| Dielectric Loading factor | 0.79 ⎫ As defined by Tien[8] |
| Impedance Reduction factor | 0.4 ⎭ |

IV. Electron Gun

Gun type — Converging Pierce Gun
Cathode type — Sprayed oxide
Cathode Current Density 213 ma/cm² (for$I_K$ = 40 ma)
Cathode diameter — 192 mils
Convergence half angle 12° 40′
Cathode radius of curvature $(\overline{r_c})$ 438 mils
Anode radius of curvature $(\overline{r_a})$ 190 mils
$\overline{r_c}/\overline{r_a}$ 2.3

Perveance 0.3 × 10⁻⁶ amps/volts³/²
$\sqrt{V_A/T_K}$ = 1.61 for $T_K$ = 720°C
At the beam minimum in absence of magnetic field:

| | | |
|---|---|---|
| $r_{min}$ (from Pierce[10]) | 11.5 | mils |
| $r_{95}/r_c$ ⎱ | 0.220 | |
| $r_{95}$ ⎰ from Danielson, Rosenfeld & Saloom[2] | 20.5 | mils |
| $r_e/\sigma$ | 3.50 | |
| $\sigma$ | 4.80 | mils |
| Brillouin flux density for 80 mil helix ID | 240 | gauss |
| Actual focusing flux density required | 600 | gauss |
| Beam transmission from cathode to collector at 5 watts output | 99% | |

V. RF Performance

| | | |
|---|---|---|
| Frequency range | 5925–6425 | mc |
| Saturation power output | 12 | watts |
| Nominal power output | 5 | watts |
| Gain at 5 watts | 31–35 | db |
| Noise figure | <30 | db |
| Input VSWR | <1.1 | ⎱ impedance match to WR 159 |
| Output VSWR (at 5 watts) | <1.4 | ⎰ waveguide |

For an explanation of symbols see page 1345.

that tube life in excess of 10,000 hours was possible with such a cathode. Moreover, an electron gun of the required convergence (about 13° half angle) could be designed using standard techniques.

The various dimensions, parameters, voltages and currents involved in the design of the MI789 are summarized in Table I. For the sake of completeness, some rf performance data are also included.

## III. DESCRIPTION OF THE TUBE

### 3.1 *General Description*

This section describes the mechanical structure of the MI789 and presents some performance data closely associated with particular portions of the tube. The overall rf performance is reserved for consideration in the next section. In the MI789 we have tried to achieve a design which could be easily modified for experimental purposes and which would also be adapted to quantity production. To assist in obtaining low gas pressure, a rather "open" structure is used, thereby minimizing the pumping impedance. In addition, all parts are designed to withstand comparatively high temperatures during outgassing, both when the tube is pumped and, in the case of the helix and gun assemblies, during a vacuum firing treatment prior to final assembly. Fig. 3 shows an MI789 and its subassemblies. Fig. 4 shows a simplified drawing of the whole tube and Fig. 5 shows how the tube is mounted with respect to the permanent magnet circuit and to the waveguides. The permanent magnets are shown schematically in Fig. 5. In actual practice they are shaped so as to produce a uniform field between the pole pieces. The means of doing this was discussed by M. S. Glass at the Second Annual Meeting of the I.R.E. Professional Group on Electron Devices, Washington, D. C., October 26, 1956.

### *Control of Positive Ions*

Our experience with previous TWT's has indicated that an improvement in life by as much as a factor of ten is obtained by arranging the dc potential profile so that positive ion bombardment of the cathode is minimized. This improvement has been observed even in tubes in which all reasonable steps have been taken toward minimizing the residual gas pressure. From Table I it is seen that the relative values of accelerator, helix, and collector voltage are arranged to drain positive ions formed in the helix region toward the collector. These ions are thereby kept from reaching the cathode. Spurious ion modulation which can result from accumulation of ions in the helix is also prevented.[1]

COLLECTOR

HELIX

UNITARY GUN – HELIX – COLLECTOR ASSEMBLY
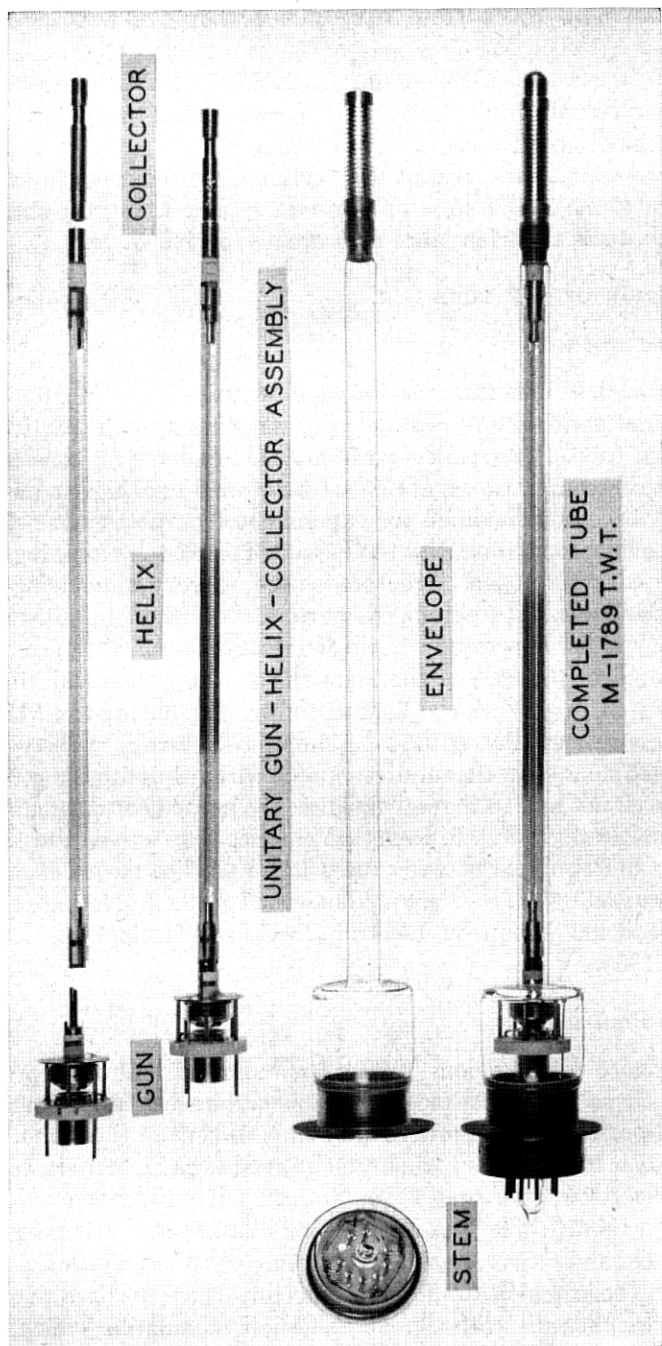
ENVELOPE

COMPLETED TUBE
M-1789 T.W.T.

GUN

STEM

Fig. 3 — The M1789 TWT and its subassemblies. In assembling the tube, the gun is first connected to the helix-collector subassembly. This unit is then inserted into the envelope and an rf braze is made between the inner collector cylinder which is part of the helix assembly and the cooling fins which are part of the envelope. This braze extends for the entire length of the fins. Finally, the stem leads are connected to the gun and a second rf braze is made between the stem and the envelope.

**GUN**   **HELIX**   **COLLECTOR**

COPPER COLLECTOR

COOLING FINS

KOVAR

REFERENCE SURFACE

INSULATOR

COUPLER FOR RF MATCHING

CERAMIC SUPPORT ROD FOR HELIX

HELIX WINDING

ACCELERATOR

INSULATOR

GLASS BULB

BEAM-FORMING ELECTRODE

CATHODE

REFERENCE SURFACES

KOVAR BULB

TUBULATION

BRAZED JOINT BETWEEN STEM ASSEMBLY AND BULB

11.2"
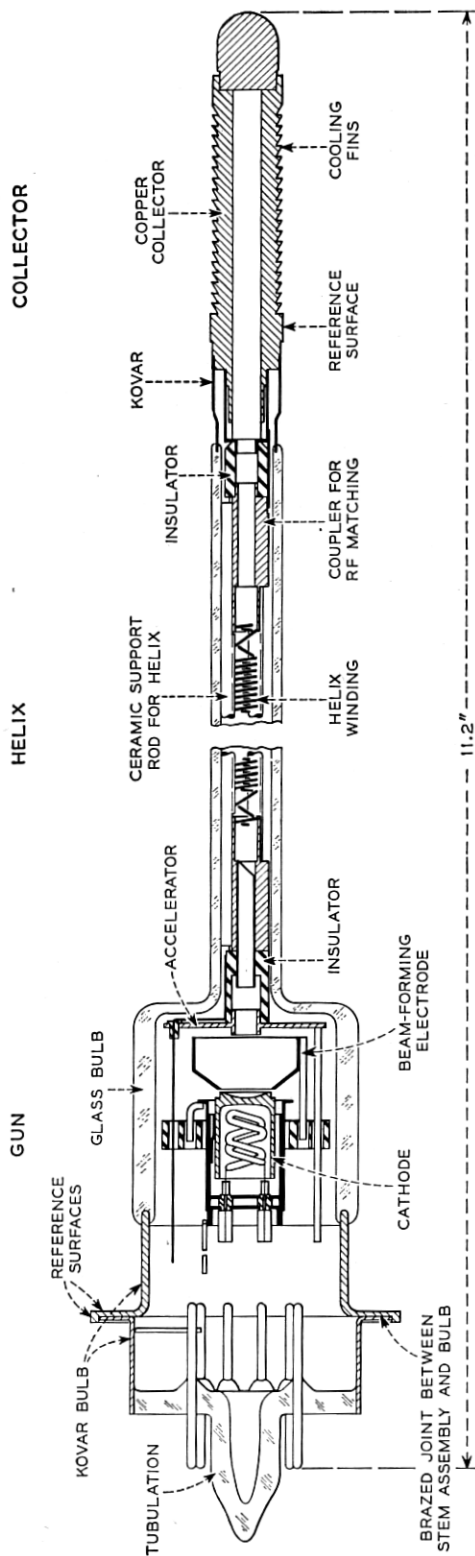
Fig. 4 — Simplified layout of the M1789. Detailed drawings of the various parts of the tube are shown in Figs. 8, 14 and 21.

The alignment surfaces are provided for mounting the TWT with respect to its associated magnetic circuit as shown in Fig. 5. These surfaces are accurately concentric with the gun helix-axis. This is accomplished by shrinking the envelope in the helix region onto a precision mandrel and then grinding the surfaces concentric with this mandrel. The helix assembly is made a close fit inside of the glass envelope (less than two mils clearance), thereby making the helix axis concentric with the alignment surfaces. The gun is aligned with respect to the helix by telescoping cylinders which are held to a clearance of less than one mil.

The ceramic insulators at the ends of the helix provide rf isolation of the helix from the gun and collector. These insulators have a larger inside diameter than do adjacent metal parts to prevent them from charging as a result of electron bombardment. We have not observed any effects in the M1789 which could be attributed to charging of these ceramics.
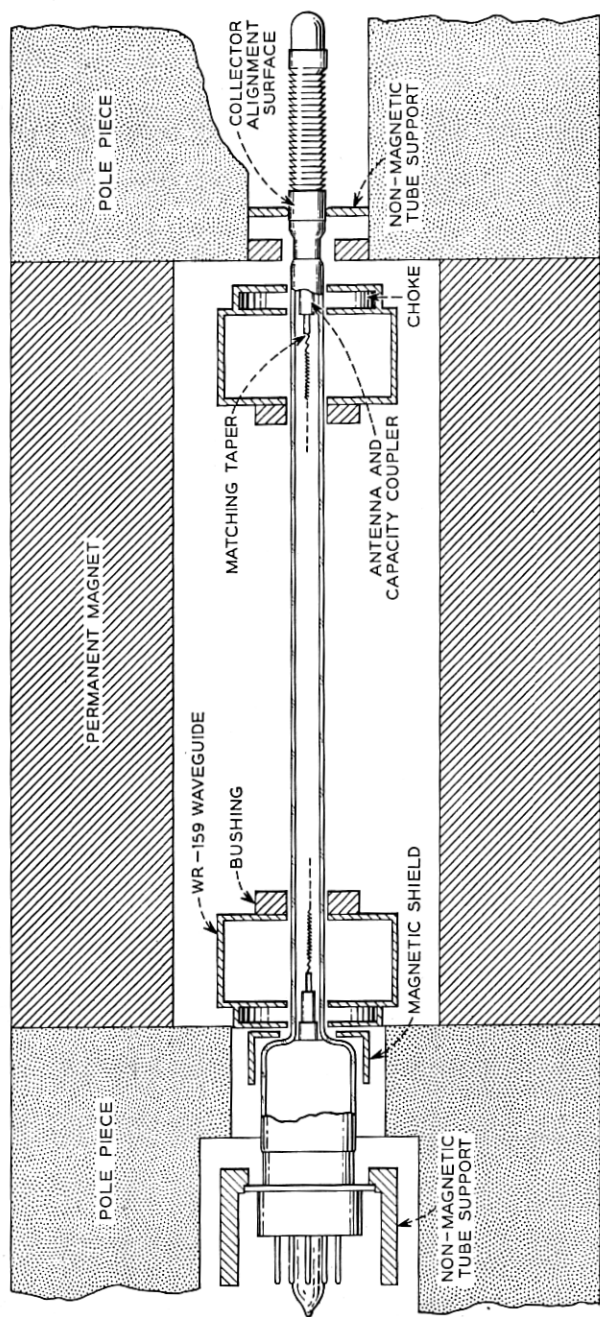
Fig. 5 — Schematic drawing of relationship of TWT to magnetic circuit and to waveguides. Mounting the gun and collector inside of holes through the pole pieces shields them from the magnetic focusing field. The helix passes through the center of the broad face of the waveguide. Energy is coupled between helix and waveguide by means of antennas and of matching tapers (see Fig. 14) at the ends of the helix. A shorting plunger is located in the waveguide about $\frac{1}{8}$ wavelength behind the TWT. The diameter of the cooling fins on the collector end is such that they can pass through the holes in the waveguide when the tube is inserted into the circuit. Forced air cooling of the collector is employed.

The effect that ions can have on cathode life was clearly demonstrated in a TWT which was in many aspects a prototype of the MI789. This tube operated with the accelerator, helix and collector at successively higher voltages, with consequent ion draining toward the cathode. Severe ion bombardment of the cathode brought about failure of most of these tubes in from 500 to 2,000 hours. In contrast to this the average life of the M1789 is in excess of 10,000 hours in spite of a cathode current density about twice that in the prototype tube. Moreover, failure of the M1789 comes about from exhaustion of coating material rather than as a result of ion bombardment. During the course of the work of the prototype tube, an experiment was performed to determine how much the ion bombardment would be affected by changing the potential difference between tube electrodes. In this experiment a small hole was drilled in the center of the cathode and an ion current monitoring electrode placed behind it. The ion monitor current was then investigated as a function of electrode voltages. Fig. 6 shows the results. We see that comparatively small potential differences are adequate to control the flow of positive ions.

### 3.2 *The Electron Gun and Electron Beam Focusing*

The electron gun used in the MI789 is a converging Pierce gun. The values of the gun parameters are summarized in Table I. Included are both the original parameters introduced by Pierce as well as those defined in a recent paper by Danielson, Rosenfeld and Saloom[2] in which the effects of thermal velocities are considered. Fig. 7 shows a drawing of the electrically significant contours of the MI789 gun. Fig. 8 shows the completed electron gun assembly. The method of constructing the gun is a modification of a procedure used in oscilloscope and television picture tubes. The electrodes are drawn parts made of molybdenum or, in the case of the cathode, of nickel. They are supported by rods which are in turn supported from a ceramic platform to which these rods are glazed. The whole gun structure is supported from the end of the helix by the helix connector detail. Since this part must operate at helix potential, it is insulated from the remainder of the gun by a ceramic cylinder which is glazed both to it and to the accelerator.

To obtain good focusing, the cathode must be accurately aligned with respect to the other electrodes. However, it must be omitted from the gun during the glazing process and during a subsequent vacuum outgassing because the cathode coating cannot withstand the temperatures involved. To insure proper placement of the cathode in the gun assembly
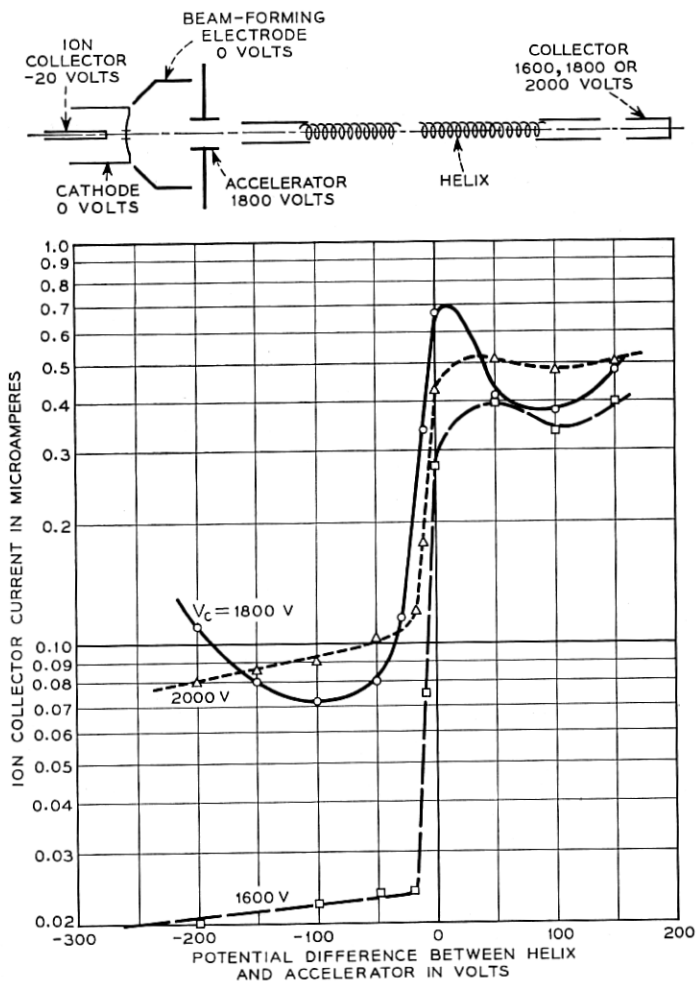
Fig. 6 — Effect of electrode voltages on ion bombardment of the cathode in a prototype of the M1789. In this experiment the helix voltage was varied while the positive ion current to a monitor electrode behind a hole in the cathode was measured. Curves are shown for the collector voltage greater than, equal to, and less than the accelerator voltage. During this experiment the accelerator voltage was held constant at 1800 volts with a resulting beam current of 40 ma. The experiment was performed on a continuously pumped system with the pressure maintained at $2 \times 10^{-7}$ mm Hg. The helix ID was 80 mils, the cathode diameter 300 mils, and the cathode hole diameter 20 mils. These curves show that the ion bombardment of the cathode can be reduced by as much as a factor of 20 by properly arranging the voltage profile.

at a later stage, an alignment cylinder is included in the gun at the time of glazing (outer cathode alignment cylinder in Fig. 8). When the gun is ready to receive the cathode, the subassembly shown in Fig. 9 is slid into the outer alignment cylinder. The cathode to beam forming electrode spacing is set using a toolmakers microscope, and welds are made between the inner and outer alignment cylinders.

Initially, we thought that the cathode should be completely shielded from the magnetic field, and that the field should be introduced in the region between the accelerator and the point at which the beam would reach its minimum diameter in the absence of magnetic field. This ar-
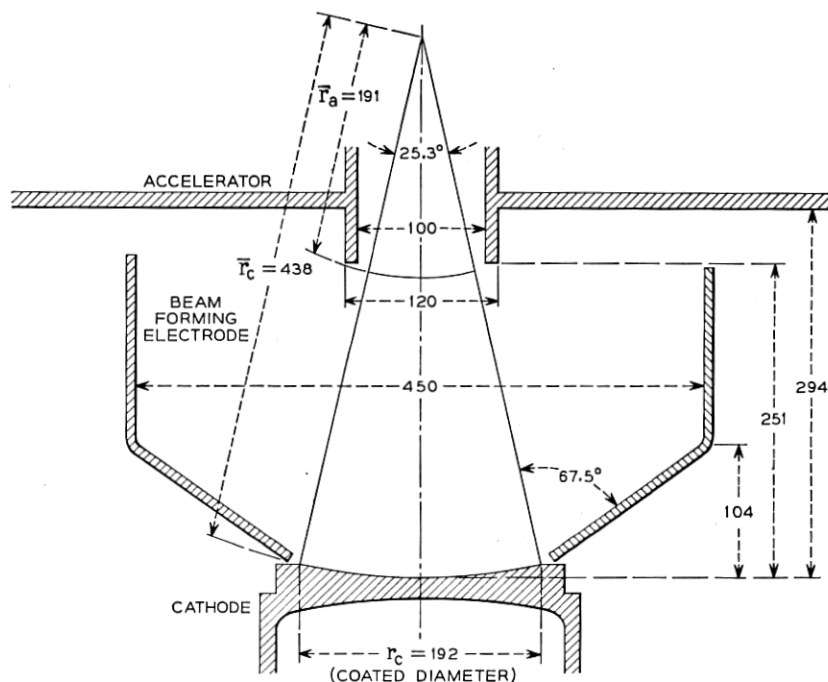


Fig. 7 — The electrically significant contours of the M1789 gun. All dimensions are in mils. These contours were determined using an electrolytic tank and following the procedure originated by Pierce. The measured potential at the beam boundary in the tank was made to match the calculated value within $\pm\frac{1}{4}$ per cent of the accelerator voltage to within 10 mils of the anode plane. The aperture in the accelerator was made sufficiently large so that substantially no beam current is intercepted on it. The significant parameters of this gun are:

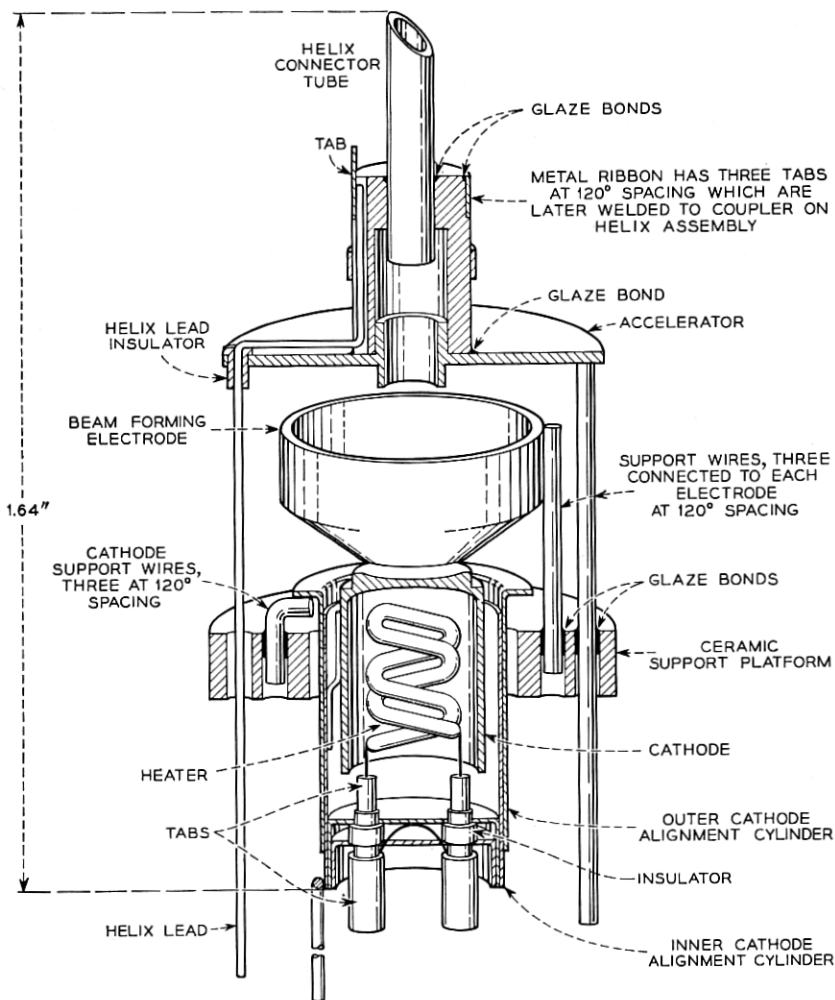| | | | | | |
|---|---|---|---|---|---|
| $P$ | $= 0.3 \times 10^{-6}$ amps/volts$^{3/2}$ | | $r_e/\sigma$ | $= 3.50$ | At the beam mini- |
| $\bar{r}_c/r_a$ | $= 2.30$ | | $\sigma$ | $= 4.80$ mils | mum in absence of |
| $\theta$ | $= 12.67°$ | | $r_{95}$ | $= 20.5$ mils | magnetic field |
| $\sqrt{V_A/T_k}$ | $= 1.61 (T_k = 720°C)$ | | $J$ | $= 213$ ma/cm$^2$ | |

Fig. 8 — M1789 electron gun assembly. In constructing the gun, all the parts with the exception of the cathode, heater, and inner support cylinder are mounted on a mandrel which fixes their relative positions. Glass powder is applied to the areas where glazed joints are desired. The unit is then heated in forming gas (85% $N_2$, 15% $H_2$) to 1100°C to melt the glass and form the glazed bonds. With this technique the precision required for alignment and spacing of the electrodes resides entirely in the tools. The helix connector tube later slides into the coupler detail of Fig. 14 to align gun and helix assemblies. The inner and outer cathode alignment cylinders are welded together at two points at the end remote from the cathode. Optical comparator inspection shows that the significant dimensions of these guns are held to a tolerance of less than ±2 mils.

rangement did result in the best beam transmission to the collector. We later discovered, however, that the noise on the electron stream became extremely high when there was no magnetic flux at the cathode. This effect will be discussed further in Section IV. We found that by having a flux density of about 20 gauss at the cathode, the noise figure could be considerably reduced with the only penalty being a slight increase in interception on the helix. The penalty results from the fact that the flux linking the cathode causes a reduction in the angular velocity of the electrons in the helix region (from Busch's theorem), and this in turn diminishes the magnetic focusing force.

Fig. 10 shows the distribution of axial magnetic field in the gun region. The curve represents a compromise between that which gives best focusing (zero flux density at the cathode) and that which gives best noise performance (about 25 gauss flux density at the cathode). This flux density variation was arrived at by empirical methods.
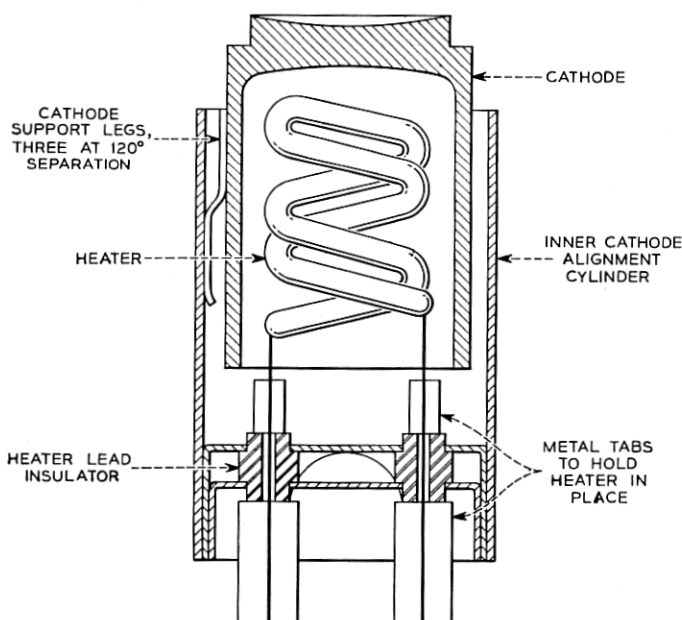


Fig. 9 — The cathode subassembly. In this unit the cathode is connected to the inner alignment cylinder by three legs. These legs are first welded to the cathode and then oven brazed to the alignment cylinder. During the brazing, a jig holds the cathode accurately concentric with this cylinder. The cathode is then coated and the unit is ready for assembly into the gun. The heater power required to raise the cathode to its operating temperature of 720°C is about six watts.

Meaurements of beam interception as a function of magnetic flux density are shown for several beam currents in Fig. 11. These measurements were obtained without any rf input to the TWT. An interesting way of normalizing these data is shown in Fig. 12. Here the magnetic
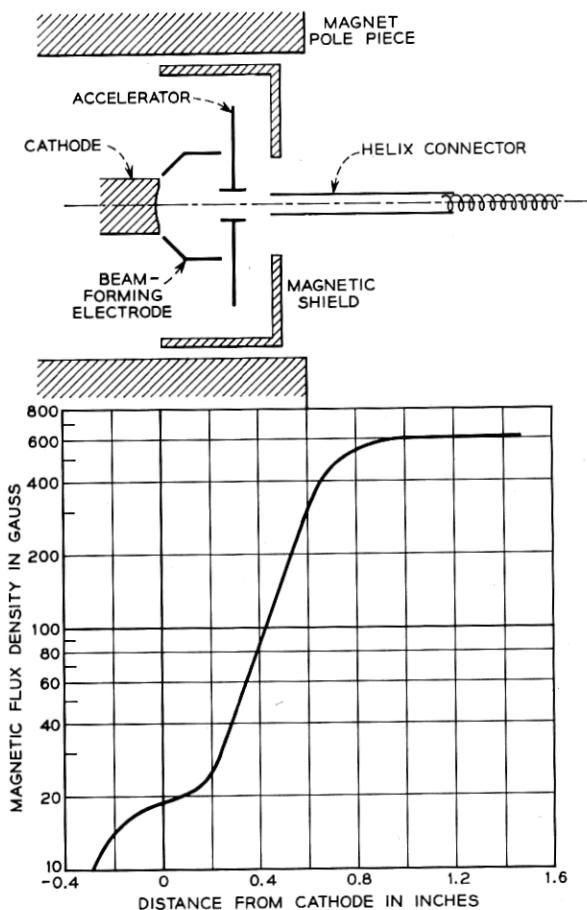


Fig. 10 — Variation in magnetic flux density as a function of distance from the cathode. A schematic representation of the gun electrodes and of the magnetic parts which have been used to control the flux is also shown. All the elements inside the tube are non-magnetic so that the flux density variation is determined entirely by magnetic parts external to the tube envelope. The flux density at the cathode is built up (i.e., the step is put into the curve) by having the magnetic shield end near the cathode. The flux which leaves the shield at this point increases the flux density at the cathode over what it would be if the shield extended well behind the cathode.

flux density has been divided by the Brillouin flux density for a beam entirely filling the helix. This quantity is the minimum flux density which could theoretically be used to focus the beam. This normalization tends to bring all of the curves together. Thus we see that, although the conditions in the MI789 are far from those of ideal Brillouin flow (because of transverse thermal velocities, aberrations in the gun, and magnetic field at the cathode), the concept of the Brillouin flux density still retains meaning, i.e., it appears that the flux density required maintains a fixed ratio to the Brillouin value.

Applying sufficient rf input to the MI789 to drive it into non-linear operation, results in defocusing caused by the high rf fields (both from the helix wave and from space charge) near its output end. Fig. 13 shows how the beam interception for different magnetic flux densities varies as a function of the power output of the TWT. From these curves we see that an output level of five watts can be maintained with about one per cent interception with a flux density of 600 gauss.
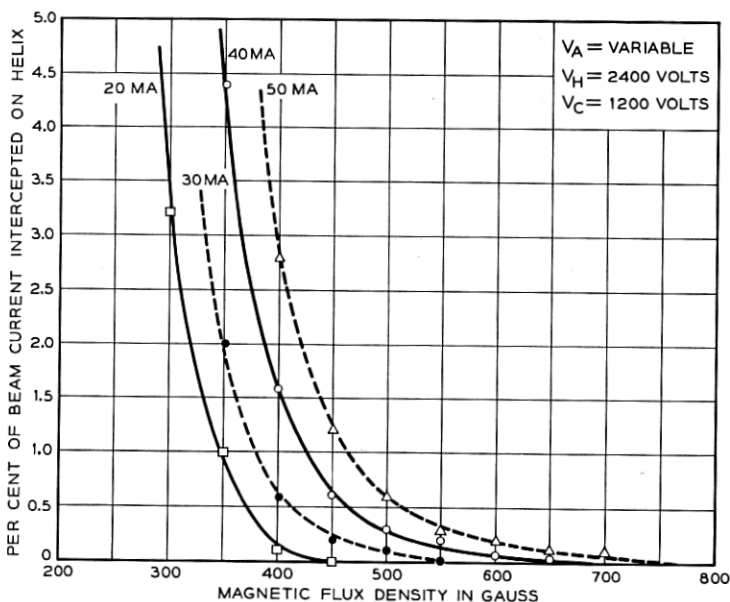


Fig. 11 — Per cent interception on the helix as a function of magnetic flux density. These measurements were taken using a precision solenoid to focus the TWT. The component of field perpendicular to the TWT axis was less than 0.1 per cent of the longitudinal field. During these measurements there was no rf input to the TWT and there was substantially no (<0.1 ma) interception on the accelerator electrode.

3.3 *The Helix*

The MI789 helix assembly is a rigid self-supporting structure composed of three ceramic support rods bonded with glaze to the helix winding. A drawing of the helix assembly is shown in Fig. 14. The support rods are made from Bell Laboratories F-66 steatite ceramic. This material was chosen because of its low rf losses and because these losses do not increase rapidly with temperature. Fig. 15 shows an enlarged photograph of the glaze bonds between the winding and one of the support rods. Attenuation is applied over a length of two inches starting 1½ inches from the input end by spraying the helix assembly with aquadag (carbon in water suspension) and then baking it.

Supporting the winding by glazing it to ceramic support rods has the following advantages:
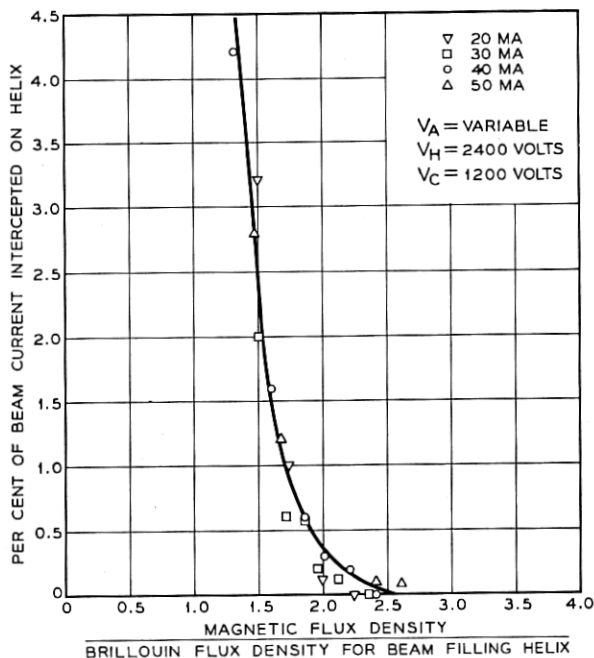


Fig. 12 — The measurements of Fig. 11 normalized in terms of the Brillouin flux density for a beam entirely filling the helix. The fact that the curves tend to come together indicates that the concept of the Brillouin flux density retains some meaning in the M1789. Because of the additional defocusing effects encountered when the M1789 is driven to high output levels, the tube is usually used with about 2.6 times the Brillouin flux density.

(1) The dielectric loading and intrinsic attenuation of the helix are comparatively low because the amount of supporting structure in the rf fields is small.

(2) High loss per unit length in the helix attenuator is made possible. The reason for this will be discussed further below.

(3) The heat dissipation capability of the helix is greatly increased because the glaze provides an intimate thermal contact between winding and support rods. This is illustrated by Fig. 16 which compares the heat dissipation properties of glazed and non-glazed helices.

(4) Mechanical rigidity is realized and therefore the helix can be handled without risk of disturbing the pitch or diameter of the winding.

On the other hand, use of the ceramic rods in the MI789 has a significant disadvantage in that it makes the outside radius of the vacuum envelope large compared to the helix radius, thus making coupled helix matching out of the question. However, since the MI789 is required to match over less than a 10 per cent band, this is not particularly serious.

To obtain reproducibility of performance in the MI789, the helix must be precisely constructed. Together, the pitch of the helix and the amount of dielectric loading determine the synchronous voltage. A pitch variation of $\pm 1$ per cent results in a voltage variation of about $\pm 50$ volts, and a loading variation of $\pm 1$ per cent results in a variation
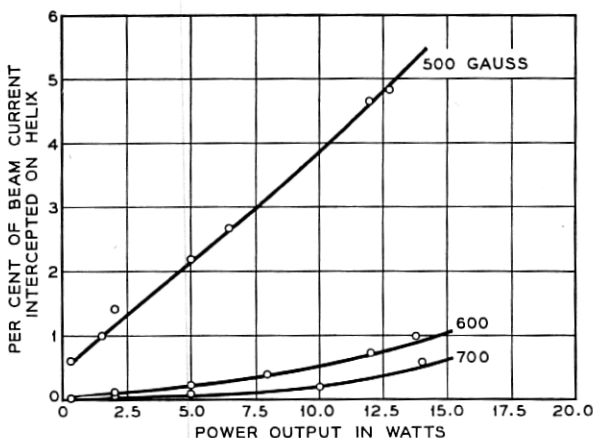


Fig. 13 — Per cent interception on the helix as a function of rf power output. These measurements were made using permanent magnet circuits charged to different field strengths. The magnetic field variation as a function of distance from the cathode was as shown in Fig. 10. The component of magnetic field perpendicular to the tube axis in these circuits was less than 0.2 per cent of the longitudinal field. All measurements were taken with a beam current of 40 ma and with the helix voltage adjusted to maximize the power output.
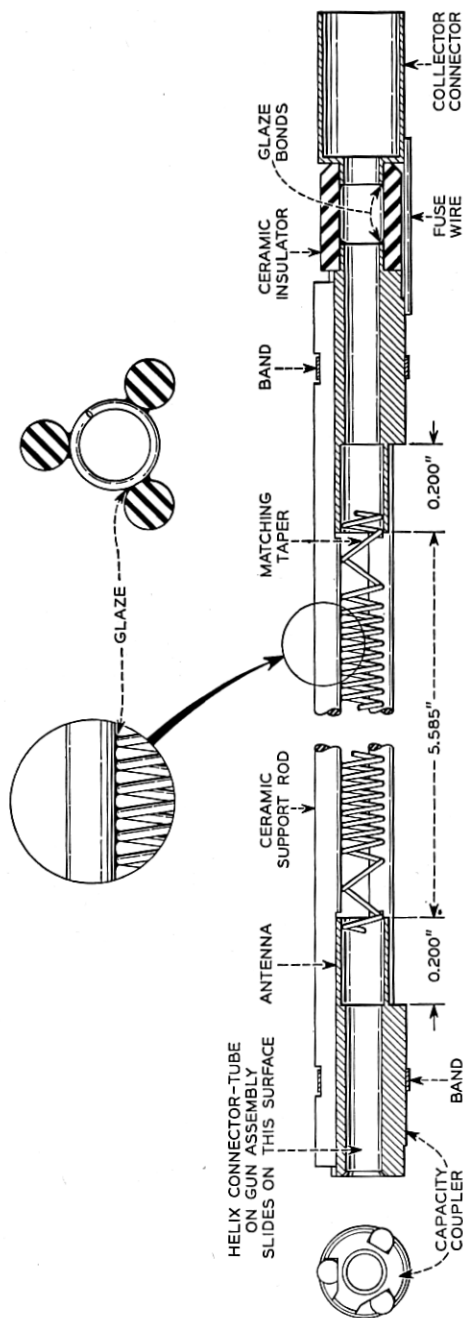
Fig. 14 — Helix assembly. The winding is supported from three F-66 ceramic rods to which it is glazed. On each end of the winding there are two turns with greater than nominal pitch to assist in transferring energy between helix and waveguides. The bands around the assembly are for the purpose of holding the support rods against the capacity couplers. There is no glaze in this region. The relationship of the antenna and capacity coupler to the waveguide circuit is shown in Fig. 5. The collector is later brazed inside of the collector connector cylinder. The fuse wire allows the helix to be heated on the pump station by passing current from the helix pin on the tube base to the collector. After outgassing the helix, the fuse is blown to isolate helix from collector. Before adding the helix attenuation, the rf loss of the helix is 3.6 ± 0.2 db. After adding the attenuation, it is 65 to 80 db. The synchronous voltage is 2200 ± 50 volts.

of about ±25 volts. It is not difficult to hold the average pitch variations to less than ±1 per cent. The loading, however, is a more difficult problem for not only must the dielectric properties of the support rods and of the glaze material be closely controlled, but attention must also be paid to the size and density of the glaze fillets. The gain of the tube is affected by the amount of loss in the helix attenuator. For the particular loss distribution used in the MI789 a variation of ±5 db out of a total attenuation of 70 db results in a gain variation of about ±1 db. The helix attenuator depends to a large extent on a conducting "bridge" between helix turns and therefore the amount of attenuation is sensitive to the size and the surface condition of the glaze fillets. Thus, the glazing process must be in good control in order to minimize variations in both gain and operating voltage. With our present techniques, we are able to hold the voltage for maximum gain to within ±50 volts of the nominal value. The gain is held to ±2 db — about half of the spread we believe to be caused by variations in loss distribution and about half by differences in beam size.
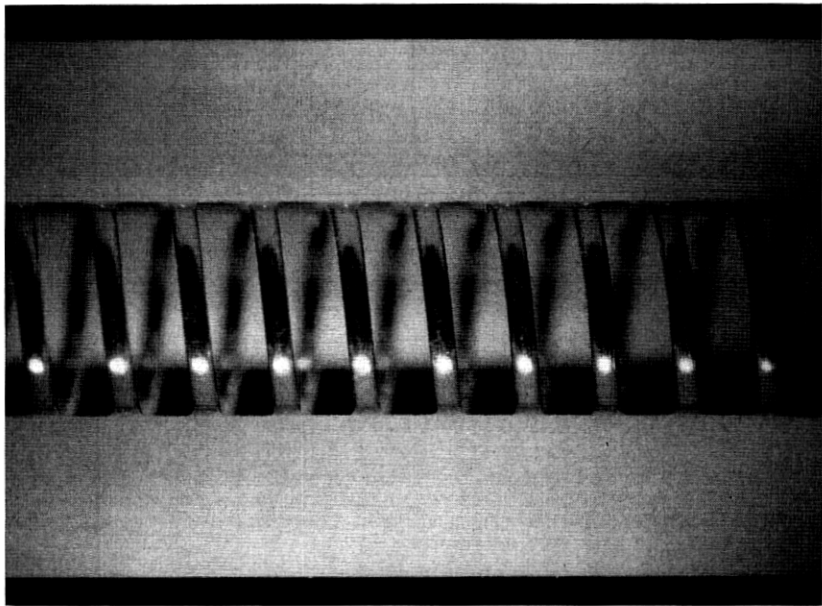


Fig. 15 — Enlarged photograph of part of an M1789 helix. Two of the ceramic support rods can be seen. The other is directly opposite the camera behind the helix and is out of focus. The fillets of glaze which bind the helix to the rods can be seen along the upper rod. This section of helix was free from applied loss.

*Helix-to-Waveguide Matching*

In the helix-to-waveguide transducer the helix passes through the center of the broad face of the waveguide and energy is coupled between helix and waveguide by an antenna and matching taper. A capacitive coupler on the helix and an rf choke on the waveguide place an effective ground plane at the waveguide end of the antenna. The rf choke also assists in minimizing leakage of rf power. Details of this transducer are shown in Figs. 5 and 14.
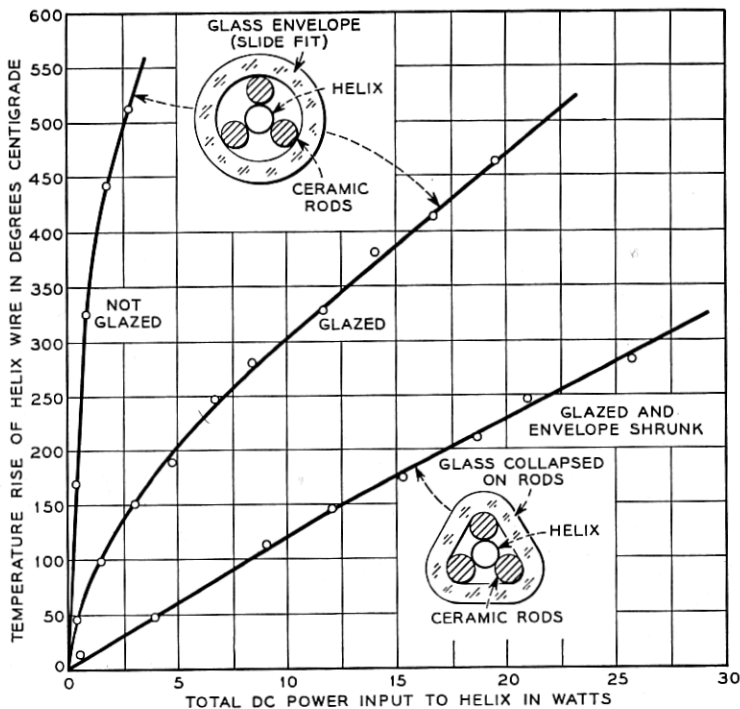


Fig. 16 — Comparison of heat dissipation properties of different helix structures. In this experiment, the helices were heated by passing dc current through them while they were mounted in a vacuum. The temperature was determined from the change in helix wire resistance.

Along with the results for glazed and non-glazed helices in a normal round envelope, this figure shows results on a structure consisting of a glazed helix in an envelope which has been shrunk around the helix support rods. This technique produces a structure which, by virtue of the good thermal contact between the support rods and the envelope, can dissipate more power than the conventional structure. The additional complication of shrinking the envelope is not necessary for the power levels used in the M1789. However, this method could be used if it were necessary to extend the tube's output range to higher power levels.

The dimensions of this transducer were determined empirically. It was found that the antenna length affects mainly the conductive component of the admittance referred to the plane of the helix. The length of the matching taper affects mainly the susceptive component, and the distance from helix to a shorting plunger, which closes off one end of the waveguide, affects both components. If for each tube, the position of the waveguides along the axis of the TWT and the position of the shorting plunger are optimized, the VSWR of the transducers will be less than 1.1 (∼26 db return loss) over the entire 500-mc frequency band. With these positions fixed at their best average value, the VSWR will be less than about 1.3 (∼18 db return loss).

### Internal Reflections

A problem that has required considerable effort has been that of "internal reflections." By this we mean reflections of the rf signal from various points along the helix as contrasted with reflections from helix-to-waveguide transducers. The principal sources of internal reflections are the edge of the helix attenuator and small variations in pitch along the helix. In the MI789 the pitch variations are the main source of difficulty.

The type of performance degradation caused by small internal reflections can be illustrated by the following. Consider a signal incident on the TWT output as a result of a reflection from a radio relay antenna. Except for a small reflection at the transducer, energy incident on the TWT output will be transferred to the helix, propagated back toward the input, and for the most part be absorbed in the helix attenuator. However, if there are reflection points along the helix, reflected signals will be returned to the output having been amplified in the process by the TWT interaction. Because of this amplification, even a small reflection of the backward traveling wave can result in a large reflected signal at the TWT output. In the MI789, these amplified internal reflections are considerably larger than the reflection from the output transducer. They limit the overall output VSWR to about 1.4, whereas the transducer alone has a VSWR of about 1.1.

If there is a long length of waveguide between the TWT and the antenna, the echo signal resulting from a reflection at the antenna and a second reflection at the TWT will vary in phase with respect to the primary signal as frequency is changed. This will cause ripples in both the gain and in the phase delay of the system as functions of frequency. Suppose the VSWR of the antenna is 1.2 and that of the TWT is 1.4 and the two are separated by 100 feet of waveguide. The amplitude of
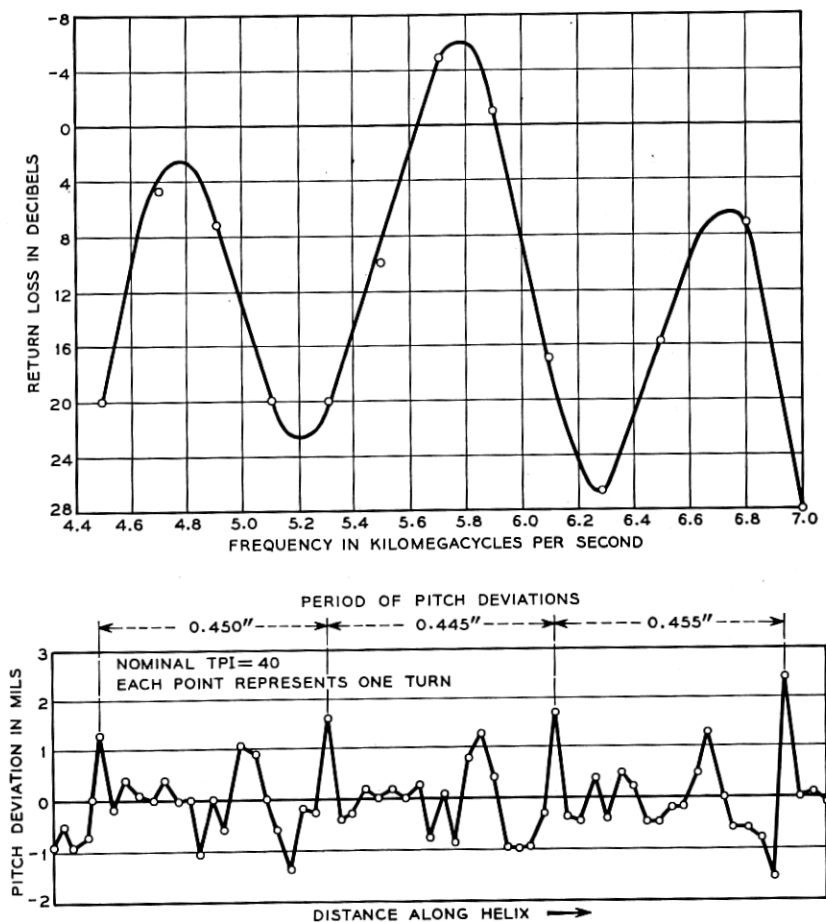
Fig. 17 — Pitch deviations and internal reflections in an early M1789 TWT. The ordinate of the pitch deviation curve is the difference between the measured spacing between helix turns and the nominal value, which for this particular helix was 25 mils. (The tube operated at 1,600 volts.) Each point represents a helix turn. It is seen that the pitch deviations are periodic in nature, repeating about every 0.450 inch.

The internal reflections were measured by matching the TWT with beam off at each individual frequency with a tuner to a VSWR of less than 1.01 (return loss greater than 40 db). The beam was then turned on and the resulting reflection taken as an approximate measure of the internal reflection. There appeared to be no appreciable change in the helix-to-waveguide transducer reflection as a result of turning the beam on. Evidence for this is the fact that when the beam was turned on with the helix voltage adjusted so that the TWT did not amplify, there was little change in the reflection.

The peaks of the internal reflection curve occur at five, six and seven half wave-lengths per period of the helix pitch deviations, indicating that the reflections from each period are adding in phase at these frequencies. At the 5,800-mc peak the return loss is positive. This indicates a reflected signal larger than the incident signal. Shorting the TWT output caused the tube to oscillate at this frequency.

the gain fluctuations will be about 0.25 db, the amplitude of the phase fluctuations will be about 0.9 degree and the periodicity of the fluctuations will be about six mc. This effect may be eliminated by using an isolator between the TWT and the antenna to eliminate the echo signal.

In addition to echo signals that occur between the TWT and the antenna there are echoes which occur wholly within the TWT as a result of a reflection of the signal from the output transducer and a second reflection from some point along the helix. Thus even if a TWT is operating into a matched load it may have ripples in gain or phase characteristics. These ripples may be controlled by minimizing the internal reflections. In the MI789 they are less than ±0.1 db in gain and one-half degree in phase. Their periodicity is about 100 mc.

In addition to causing transmission distortions, internal reflections can seriously reduce the margin of a TWT against oscillation. Outside of the frequency band of interest, the helix-to-waveguide transducer may be a poor match or the TWT may even be operating into a short circuit in the form of a reflection type bandpass filter. At such frequencies, the internal reflections must not be large enough so that an echo between transducer or filter and an internal reflection point will see any net gain, or else the TWT will oscillate.

With many types of helix winding equipment, variations in helix pitch are periodic in nature. This causes the helix to exhibit a filter-like behavior with respect to internal reflections. At frequencies at which the period of the pitch variations is an integral number of half-wave lengths, the resultant reflections from each individual period will add in phase, thereby causing the helix to be strongly reflecting at these frequencies. This effect can perhaps best be illustrated by considering some results obtained in an early stage of the MI789 development. Fig. 17 shows measurements of the spacing between turns of an early helix. Also shown is the return loss as a function of frequency that a signal incident on the output of an operating TWT would see as a result of internal reflections alone. Helix-to-waveguide transducer reflections were eliminated with waveguide tuners during this experiment. The deviations in helix pitch from nominal are rather large and are markedly periodic in nature. The resulting internal reflections show strong peaks at frequencies corresponding to five, six and seven half-wavelengths per period of the pitch deviations.

In the present MI789 this situation has been considerably improved by increased precision in helix winding and by insuring that the remaining periodicity does not produce a major reflection peak in the band. Fig. 18 shows pitch measurements and internal reflections for a recently constructed tube.
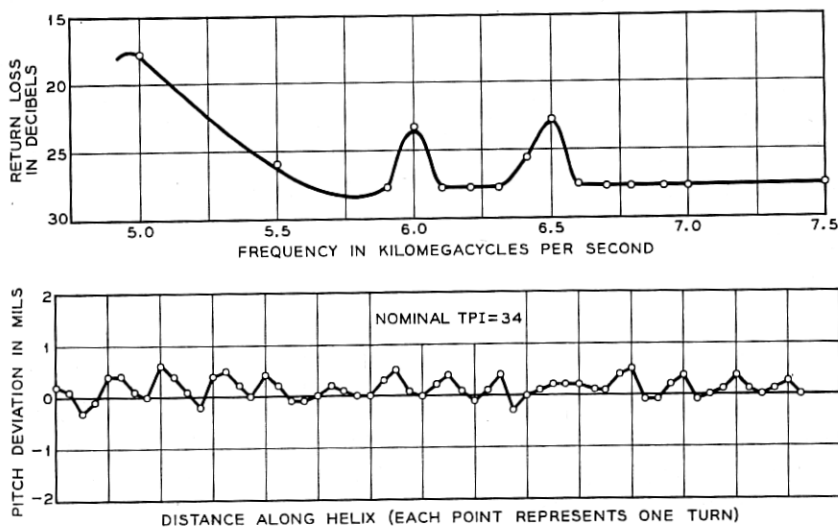
Fig. 18 — Pitch deviations and internal reflections in a recent M1789 TWT. By precise helix winding techniques the pitch deviations have been reduced by a factor of about 10 over those occurring in early tubes. The resulting internal reflections have been improved by about 25 db although there is still a residual periodicity remaining.

For return losses greater than about 25 db, we begin to see internal reflections originating from the edge of the helix attenuator. At these values of return loss, the measurements also begin to be in appreciable error as a result of the residual transducer reflections.

### Helix Attenuator

Attenuation is applied to the helix by spraying aquadag directly on the helix assembly and then baking it. The result is a deposit of carbon on the ceramic rods and on the glaze fillets. The attenuation is held between 65 and 80 db and is distributed as shown in Fig. 19. Evidently most of the loss is caused by a conducting bridge which is built up between helix turns. This was indicated by one experiment in which we cleaned the deposit off the rods of a helix by rubbing them with emery paper. Only the carbon directly between helix turns then remained. This decreased the total attenuation by less than 20 per cent. Having the helix glazed to the support rods is apparently necessary in order to get good contact between the winding and the carbon "bridge." We have been able to obtain about four times as much loss per unit length with glazed helices as with non-glazed ones. Using our method of applying attenuation we can add in excess of 80 db/inch to a glazed helix. The ability to obtain such high rates of attenuation allows us to concentrate the loss along the helix thereby minimizing the TWT length.

The machine used for spraying aquadag on the helix is shown in Fig.

20. A glass cylinder and photocell arrangement is used to monitor the amount of carbon deposited. In this manner the attenuation added is made independent of both the aquadag mixture and the nozzle setting of the spray gun. This machine has been checked alone by using it to spray glass slides which are then made into attenuator vanes. Over a two-year period we have found that a given light transmission through the monitor slide results in the same vane attenuation within ±2 db out of 40 db.

After a helix has been sprayed, it is vacuum fired at 800°C for thirty minutes and then the loss is measured. About 60 per cent of the helices fall within the desired range of 65–80 db. The principal cause of the differences in attenuation is believed to be variation in the condition of the glaze fillets. Helices not meeting specifications are sprayed and fired a second time (after cleaning off excess aquadag if necessary). This second treatment, brings the attenuation of almost all helices to within the desired range.

### 3.4 *The Collector*

It is desirable to operate the collector at the lowest possible voltage in order to minimize the dc power input to the TWT. This increases the overall efficiency and simplifies the collector cooling problem. On the
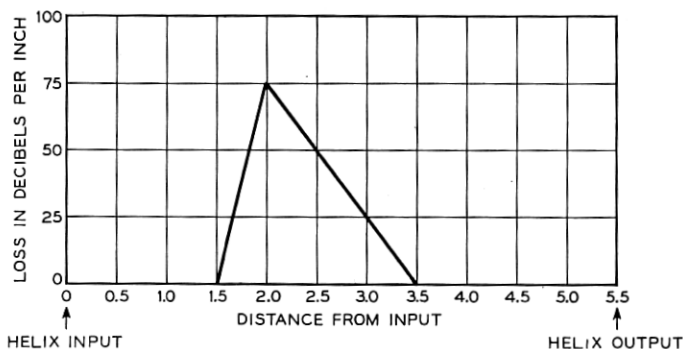


Fig. 19 — Distribution of helix attenuation. The attenuation pattern has a gradually slanting edge facing the output to provide a smooth transition into the loss for any signals traveling backwards toward the input. Reflections of these signals must be very small since the reflected signals will be amplified in the process of returning toward the output. Cold measurements (i.e., measurements on the helix without electron beam) made by moving a sliding termination inside the helix, indicate that the return loss from the attenuator output is better than 45 db, the limiting sensitivity of our measurement. The input side of the helix attenuator is also tapered to minimize reflections but this taper is much sharper than that on the output side because there is comparatively little gain between input and attenuator. Cold measurements with a sliding termination showed a return loss for this taper of about 40 db. (Surprisingly, even a sharp edge produces a reflection with a return loss of almost 30 db.)

other hand, if there is appreciable potential difference between helix and collector, we must insure that few secondary or reflected electrons return from the collector to bombard the helix and accelerator, or else we may overheat these electrodes. Fig. 21 shows a drawing of the collector used in the M1789. It takes the form of a long hollow cylinder shielded from the magnetic field. Inside of the collector the beam is allowed to gradually diverge and the electrons strike the walls at a grazing angle. This design reduces secondary electrons returned from the collector to almost negligible proportions.
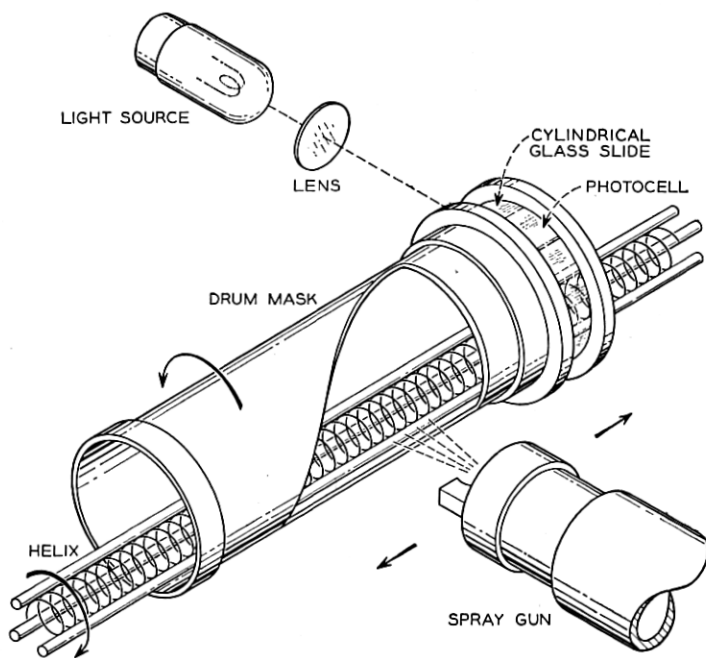
Fig. 20 — Schematic diagram of the machine used for spraying aquadag attenuation on the helix. In this machine the helix is rotated rapidly to insure uniform exposure to the spray. At the same time the masking drum rotates at a slower speed and the spray gun traverses back and forth along the masking drum. The drum therefore acts as a revolving shutter between the helix and the spray gun and its degree of opening serves to control the amount of aquadag reaching the helix. From a knowledge of the rate of attenuation increase as a function of the amount of carbon deposited (empirically determined) the shape of the drum opening can be calculated so as to give any desired attenuation pattern.

The spray gun also passes over a glass cylinder at one end of the masking drum so that it receives a sample of the aquadag spray. A photocell is used to monitor light transmitted through the cylinder. Before starting to spray, the glass is cleaned and the photocell reading is taken as 100 per cent light transmission. The helix is then sprayed until the light transmission has decreased to the proper value. The photoelectric monitoring technique makes the attenuation added insensitive to the aquadag composition and to the spray gun nozzle opening.
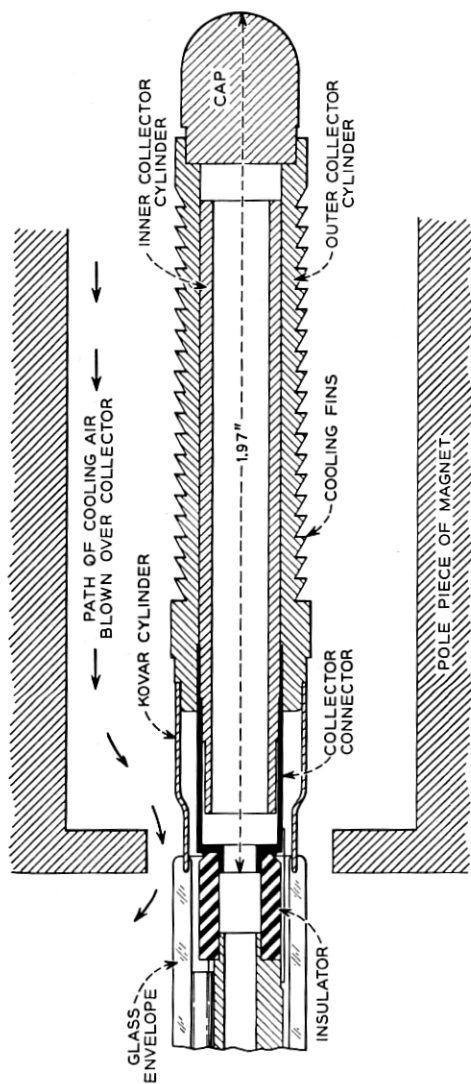
FIG. 21 — The collector consists of two cylinders. The inner cylinder is the electron collector proper and is part of the helix subassembly. The outer cylinder is part of the envelope subassembly. The two parts of the collector are brazed together in the final assembly of the tube. The collector is shown in its position with respect to the pole piece at the output end of the magnetic circuit. The magnetic field variation in the collector region is plotted to the same scale as the collector drawing. The electron beam diverges gradually inside of the collector and the electrons strike the walls at a grazing angle. With this design there are essentially no secondary electrons returned from the collector.
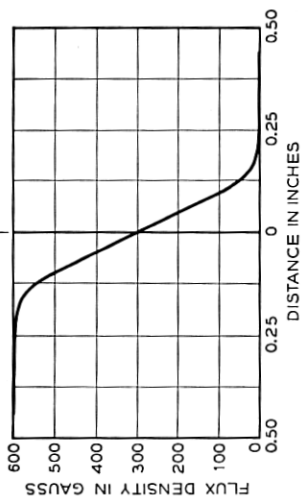
Fig. 22 shows the total accelerator and helix interception as functions of collector voltage at various output levels. When there is no rf drive, the intercepted current remains low to a collector voltage of about 200 volts at which point it suddenly increases to a high value. This appears to be caused by the phenomenon of space charge blocking. As the collector voltage is progressively lowered, the space charge density at the mouth of the collector increases because of the decrease in electron velocity at this point. Increasing the charge density causes the potential depression in the beam to increase until at some collector voltage the potential on the axis is reduced to cathode potential. At collector voltages lower than this, some of the beam is blocked, i.e., it is turned back by the space charge fields.

When the TWT is operated at appreciable rf output levels, the collector voltage must be increased to permit collection of all electrons which have been slowed down by the rf interaction. Unfortunately, some electrons are slowed far more than is the average, so that we must supply to the TWT several times more dc power than we can take from it in the form of rf power. However, as seen from Fig. 22, there is still an appreciable advantage to be gained by operating the collector at lower than helix potential. These curves should not be taken as an accurate measure of the velocity distribution because there are undoubtedly space charge blocking effects which even at higher collector voltages have some influence on the number of electrons returned from the collector. This arises from the fact that the rf interaction causes an axial bunching of the electrons, thereby causing the space charge density in an electron bunch to be much higher than it is in an unmodulated beam. Thus, as a bunch enters the collector, the local space charge density may be high enough to return some electrons.

IV. PERFORMANCE CHARACTERISTICS

4.1 *Method of Approach*

In this section we will consider the overall rf performance of the M1789 and make some comparisons between theory and observed results. The following TWT parameters can be varied: input level; helix voltage; beam current; frequency; and magnetic field. Our approach here will be to first consider the operation of the tube under what might be called nominal conditions. This will be followed by a discussion of the variations in low-level gain and in maximum output over an extended range of beam current, frequency, and magnetic field. By this procedure we are able to obtain a description of tube performance without presentation of a formidable number of curves. Two topics, noise and inter-
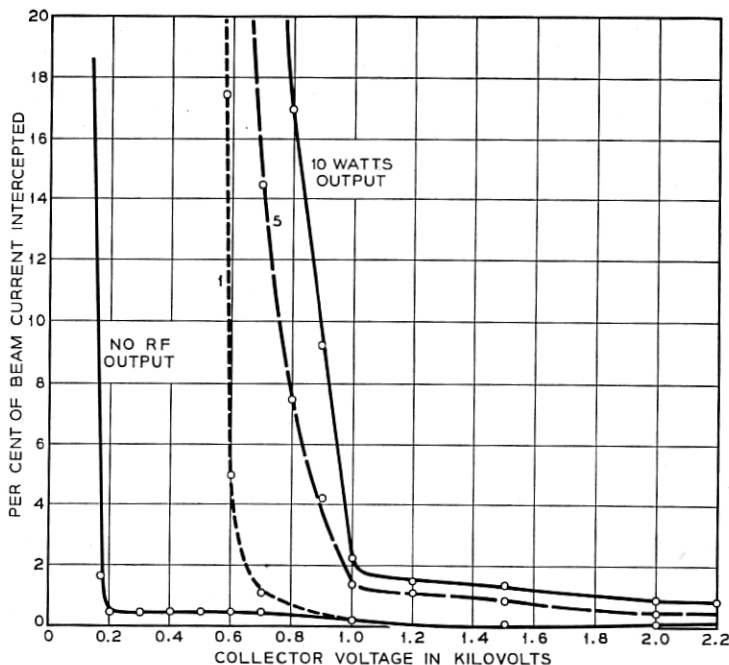
Fig. 22 — Intercepted current as a function of collector voltage with helix and accelerator voltages held constant at their nominal values. Below the knee of the curves about three quarters of the total intercepted current goes to the helix and about one quarter is focused all the way back to the accelerator. Curves are shown for no rf input and for output levels of 1, 5, and 10 watts. With no input, the lowest permissible collector voltage is determined by the phenomenon of space charge blocking. With rf input, it is determined mainly by the velocity spread of the electrons. In all cases it was found that the alignment of the TWT with respect to the magnetic circuit becomes more critical as the knee of the curve is approached. For this reason the M1789 is usually operated with a collector voltage about 200 volts above the knee.

modulation, will be divorced from the discussion as outlined above and treated separately in Sections 4.4 and 4.5.

### 4.2 *Operation Under Nominal Conditions*

*Basic Characteristics*

By nominal conditions for the M1789 we mean the following:

frequency.........................6175 mc (band center)
beam current....................................40 ma
magnetic flux density...........................600 gauss
collector voltage..............................1200 volts

Fig. 23(a) shows representative curves of output power as a function of input power for several values of helix voltage. This information is re-plotted in Fig. 23(b) in terms of gain as a function of output power. We see that the TWT operates as a linear amplifier for low output levels. As the output level is increased, the tube goes into compression and finally a saturation level is reached. The maximum gain at low input levels is obtained with a helix voltage of 2,400 volts (about 10 per cent higher than the synchronous voltage because of space charge effects).
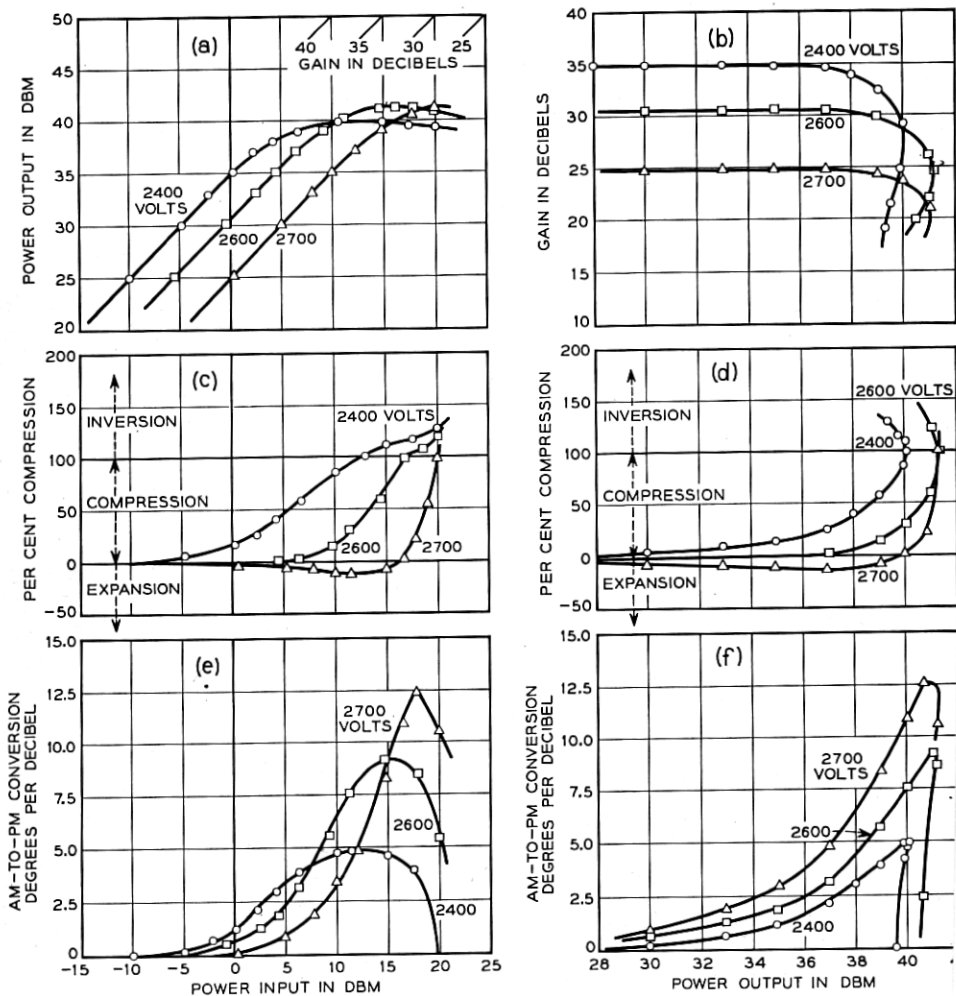
Fig. 23 — See opposite page for caption

The maximum output at saturation is obtained at a higher helix voltage as is common in TWT's. The helix voltage also affects the shape of the input-output curves — linear operation being maintained to higher output levels at higher helix voltages.

As a measure of the efficiency of electronic interaction in a TWT, we use an "electronic efficiency" which is defined as the ratio of the rf output power to the beam power (product of helix voltage and beam current). The "over-all efficiency" we define as the ratio of the rf output power to the total dc power (exclusive of heater power) delivered to the tube. With the collector operated at 1,200 volts, it is about twice the electronic efficiency. For the M1789, maximum efficiency occurs at the saturation level with a helix voltage of 2,600 volts. The electronic and over-all efficiencies there are equal to about 14 per cent and 28 per cent, respectively.

The curves of Figs. 23(a) and (b) were taken with sufficient time allowed for the tube to stabilize at each power level. If the TWT is driven to a high output level after having been operated for several minutes with no input signal, the output will be somewhat greater than is shown in the curves. It will gradually decrease until it reaches a stable level in a period of about two minutes. This "fade" is caused by an increase in the intrinsic attenuation of the helix near the output end. The increase is a result of heating from rf power dissipation. At maximum output the fade is about 0.6 db (about 15 per cent decrease in output power). At the five-watt output level the fade is about 0.1 db (about 2 per cent

---

Fig. 33 — See opposite page

(a) Output power as a function of input power. Both ordinate and abscissa are in dbm (db with respect to a reference level of one milliwatt). A straight line at 45° represents a constant gain. A gain scale is included along the top of the figure. For this tube a helix voltage of 2,400 volts gives maximum gain at low signal levels and a voltage of about 2,600 gives maximum output at saturation.

(b) Gain as a function of output power. This is an alternate way of presenting the information shown in (a).

(c) Compression as a function of input power. Three regions are shown in the figure. The "compression" region is that in which there is less than one db change in output level for a db change in input level. The "expansion" region is that in which there is more than one db change in output level for a db change in input level. The "inversion" region is that in which the output level decreases when the input level increases (or vice versa). It occurs for input levels greater than that necessary to drive the TWT to saturation. In this region the change in output is of opposite sign to the change in input. Using the definition in the text this gives rise to compression values in excess of 100 per cent.

(d) Compression as a function of output power.

(e) Conversion of amplitude modulation to phase modulation as a function of input power. This conversion arises because the electrical length of the TWT is a function of the input level. The effect can cause rather serious difficulties in certain types of low index FM systems.

(f) Conversion of amplitude modulation to phase modulation as a function of output power.

decrease in output power). We will present some additional data on this effect in Section 4.3.

### Distortion of the Modulation Envelope

The curves of Figs. 23(a) and (b) tell what happens when a single frequency carrier signal is passed through the TWT. In addition we would like to know the effect on modulation which may be present on the signal. In particular, it is desirable to know the compression of the envelope of an AM signal and the amount of phase modulation generated in the output signal as a result of amplitude modulation of the input signal, (an effect commonly known as AM-to-PM conversion). As a measure of compression of an AM signal the quantity per cent compression will be used. This is defined as

$$\% \text{ Compression} = \left[1 - \frac{\Delta V_0/V_0}{\Delta V_i/V_i}\right] 100$$

where $V_0$ is the voltage of the output wave, $V_i$ is the voltage of the input wave, and $\Delta V_0$ is the change in output voltage for a small change $\Delta V_i$ in the input voltage. When $\Delta V/V$ is small it can be expressed in db as $8.68 \Delta V/V = \Delta V/V$ in db. From this it follows that

$$\% \text{ Compression} = \left[1 - \frac{\Delta P_0}{\Delta P_i}\right\} \text{ in } db\right] 100$$

where $\Delta P_0$ is the change in output power for a change $\Delta P_i$ in input power, and the two powers are measured on a db scale. When the per cent compression is zero the TWT is operating as a linear amplifier; when it is 100 per cent the TWT is operating as a limiter.

From the above expression it may appear that the per cent compression could be determined directly from the slopes of the input-output curves. This would be the case were it not for fading effects. Since there is fading, however, the slope for rapid input level changes is different at high levels from the slope of the static curves. Thus it is necessary to determine compression from the resulting effect on an AM signal.

The electrical length of a TWT operated in the non-linear region is to some extent dependent on the input level. Therefore, an AM signal applied to the input of the TWT will produce phase modulation (PM) of the output signal. This effect may be of particular concern when a TWT operating at high output levels is used to amplify a low-index FM signal. If such a signal contains residual amplitude modulation, the TWT generates phase modulation with phase deviation proportional to the input amplitude variation. Under certain circumstances this can cause

severe interference with the signal being transmitted. We will discuss a particular example after consideration of the compression and AM-to-PM conversion characteristics of the M1789.

As in the case of compression, we must measure AM-to-PM conversion dynamically. This is necessary because point-by-point measurements of the shift in output phase as input level is changed include a component of phase shift caused by changes in temperature of the ceramic support rods and a consequent change in their dielectric constant. However, this thermal effect does not follow AM rates of interest and therefore does not produce AM-to-PM conversion.

Fig. 24 shows a simplified block diagram of the test set used to measure compression and AM-to-PM conversion. This equipment amplitude modulates the input signal to the TWT under test by a known amount and detects the AM in the output signal with a crystal monitor and the PM with a phase bridge. A more complete discussion of this measurement is given by Augustine and Slocum.[3]

Compression is given as a function of power input in Fig. 23(c) and as a function of power output in Fig. 23(d). We see that compression sets in more suddenly at higher helix voltages. Above about 2,500 volts
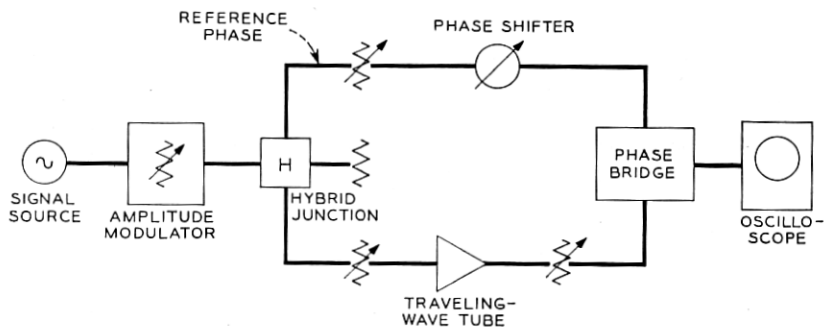


Fig. 24 — Simplified block diagram of test set used to measure compression and conversion of amplitude to phase modulation. A ferrite modulator introduces one db of 60 cps amplitude modulation into the test signal. The 60 cps rate is much higher than that which can be followed by thermal changes in the TWT. Half of the modulated signal serves as input to the TWT under test and half serves as a reference phase for a phase detector. The signals at the phase detector input are maintained equal and at constant level and nominally in phase quadrature. The detector is essentially a bridge circuit, the output of which is a dc voltage proportional to the phase difference of the two inputs. When operated with inputs in quadrature it is not sensitive to amplitude changes of as much as two db in either or both inputs. Phase modulation introduced by the amplitude modulator appears at both inputs and thus does not produce an indication. The output of the detector is therefore a direct measure of the phase modulation created in the TWT. Compression is determined by comparing the percentage amplitude modulation at the input and output crystal monitors.
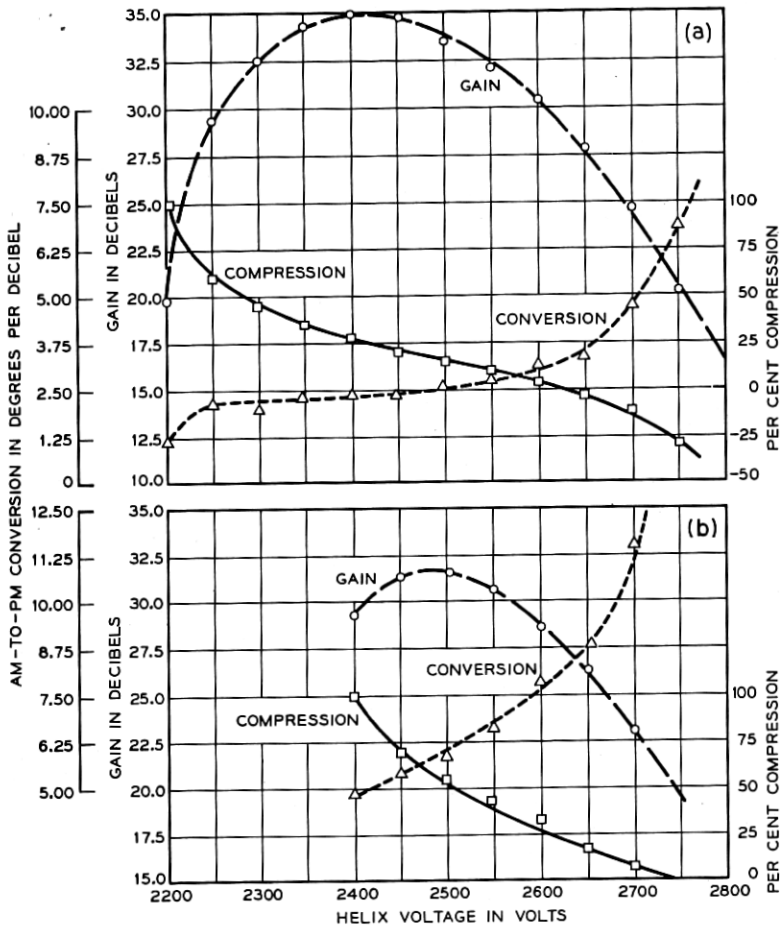
Fig. 25 — Gain, compression and amplitude to phase conversion as a function of helix voltage with the output power maintained constant at a level of five watts (a) and ten watts (b).

there is expansion for some values of power input. Figs. 23 (e) and 23(f) give the AM-to-PM conversion, as functions of input and output power respectively. These data indicate that the conversion is very much less if the tube is operated at lower helix voltages. For example, the conversion at the saturation level of the 2,700-volt curve is about $2\frac{1}{2}$ times that for the 2,400-volt curve.

A final method of plotting gain, compression, and AM-to-PM conversion data is shown in Fig. 25. The abcissa here is the helix voltage.

For these measurements power output was held constant by adjusting input level at each voltage. The figure shows that as helix voltage is increased, the compression decreases but the AM-to-PM conversion increases. The choice of a helix voltage at which to operate the tube must therefore represent a compromise between these quantities.

### Phase Modulation Sensitivity

The equipment of Fig. 24 was also used to measure the phase modulation sensitivity of various electrodes by omitting the amplitude modula-
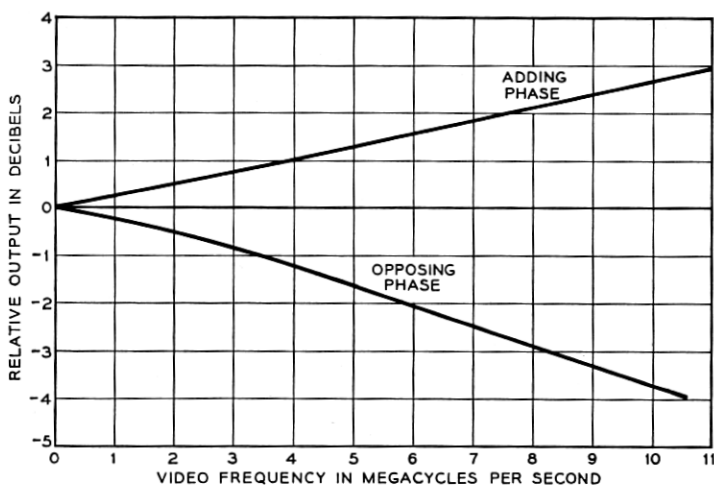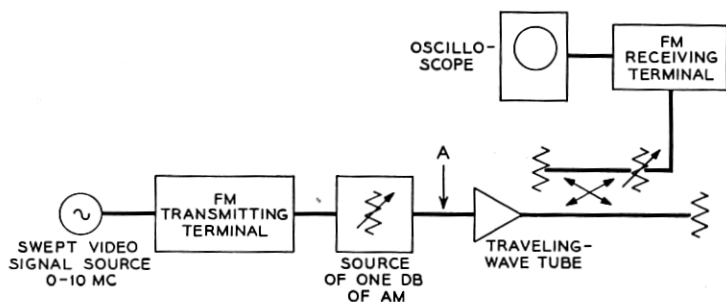


Fig. 26 — Example of frequency response shaping caused by AM-to-PM conversion. This figure shows the calculated frequency response viewed between FM terminals for the system shown in the block diagram. Curves are given for the case in which the phase modulation generated in the TWT both adds to and subtracts from that of the transmitted signal. Inclusion of a limiter at point A would result in a flat frequency response.
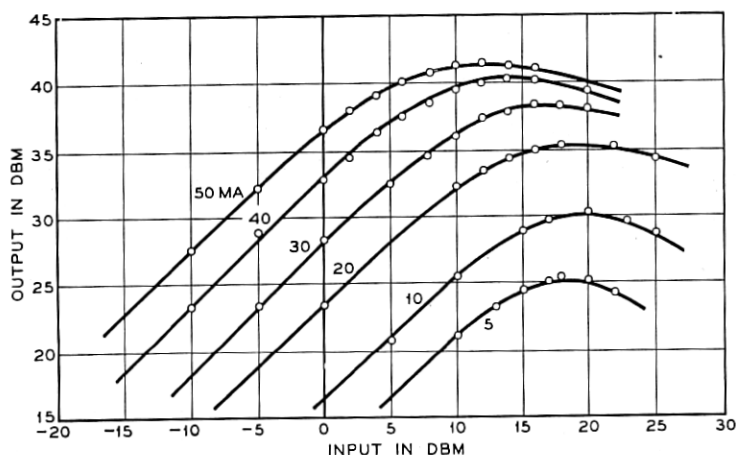
Fig. 27 — Output power as a function of input power at various beam currents. These curves were all taken with the helix voltage adjusted to give the maximum gain at low signal levels. At low beam currents (<20 ma) there is insufficient gain between the attenuator and the output so that at these currents the attenuator section is limiting the power output. This accounts for some of the difference in shape of the curves near maximum output.

tor and introducing small changes in electrode voltages. The modulation sensitivity of the helix is about two degrees per volt and that of the accelerator about 0.1 degree per volt with the TWT operating under nominal conditions.

### Significance of AM-to-PM Conversion

Let us return briefly to a discussion of some consequences of AM-to-PM conversion. As an example, we will consider the case of a low-index FM signal. Assume the frequency deviation is ±5 mc peak to peak. This gives a phase deviation of ±0.5 radian for a 10 mc modulating signal. These values are typical of what might be found in a radio relay system. Let us also assume that there is a residual amplitude modulation of one db (about 13 per cent) in this signal and suppose further that the signal is amplified by a TWT having a value of AM-to-PM conversion of 10 degrees per db. The phase modulation thus created in the TWT can either add to or subtract from that of the original FM signal, thus changing its modulation index. At low modulation signal frequencies the phase deviation of the FM signal will be large compared to that of the PM interference and the interference will be of little consequence. At high modulation signal frequencies the phase deviation of the original FM and of the interfering PM signals will be comparable and the interference

can considerably change the net phase deviation of the overall signal. For the example we are considering the frequency responses in Fig. 26 show what would be seen at the output FM terminal. Curves are given both for the PM interference adding to and subtracting from the original FM signal. We see that a gain-frequency slope of about 4 db over 10 mc is introduced by AM-to-PM conversion. To prevent such an effect, a limiter should be used prior to the TWT in applications of this nature so as to remove the offending AM from the input signal.

The fact that compression and amplitude-to-phase conversion vary with input level means that in addition to the first order distortion just described, higher order distortions of the modulation envelope will occur. If, for example, the input signal is amplitude modulated at frequency $f_1$, the output modulation envelope will contain amplitude and phase modulation both at $f_1$ and at harmonics of $f_1$. The amount of higher order distortion can be estimated by expanding the compression and amplitude-to-phase conversion curves as a function of power input in a Taylor series about the operating point. Such an expansion shows that the greater the slope of these curves the greater will be the higher order distortions.
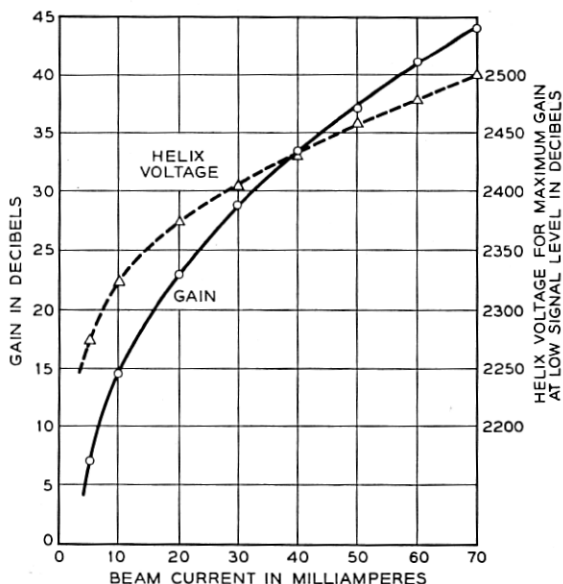


Fig. 28 — Low-level gain as a function of beam current. The helix voltage was adjusted for maximum gain at each current.

*Reproducibility*

The curves presented in this section are all for the same tube, one which is representative of a group of 50 which were built at the conclusion of the M1789 development program. The tubes in this group had characteristics falling within the following ranges. The numbers represent the range containing 90 per cent of the tubes tested.

Accelerator Voltage for 40 ma..................2,500–2,700
Helix Voltage for maximum low-level gain.......2,350–2,450
Low-level gain................................33–37 db
Gain at 5 watts output........................31–35 db
Maximum power output.................$\left\{\begin{array}{l}\text{40.5–42 dbm}\\\text{(11.2–15.8 watts)}\end{array}\right.$
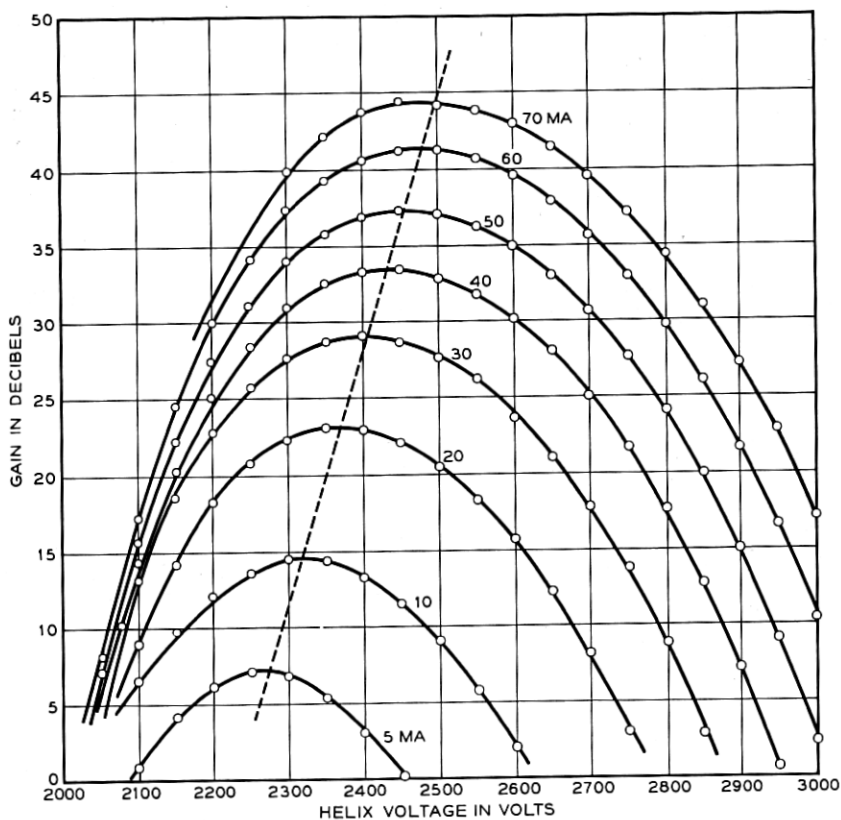


Fig. 29 — Low-level gain as a function of helix voltage for various beam currents. The dotted line represents the locus of the maxima of the curves.
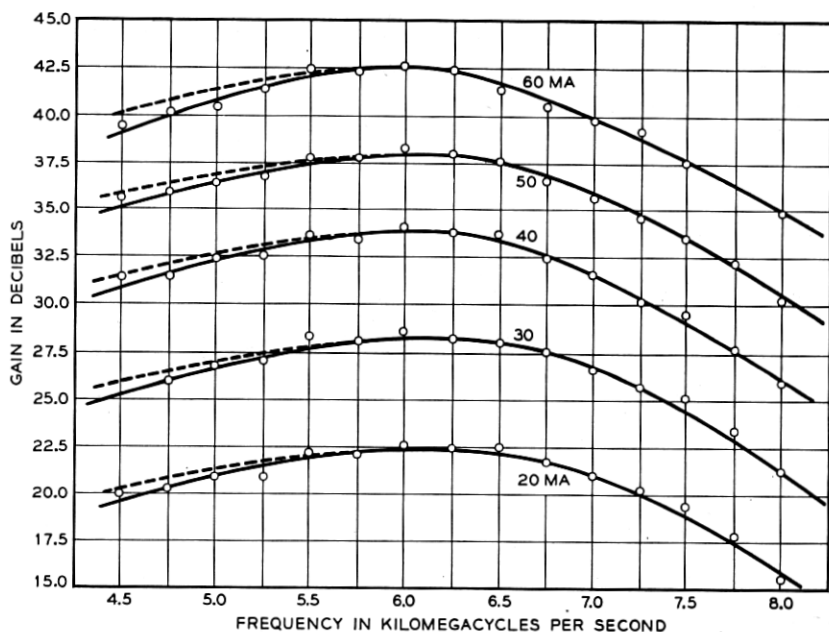
Fig. 30 — Low-level gain and helix voltage for maximum gain as functions of frequency for several beam currents. The TWT was matched to the waveguide (with tuners where necessary outside of the 5,925 to 6,425-mc range) at each frequency. The solid curves show the gain-frequency characteristic with the helix voltage adjusted for maximum gain at 6,000 mc for each beam current and then held constant as frequency was changed. Experimental points correspond to this condition. The dotted curves show how the characteristics change when helix voltage is optimized at each frequency. The optimum helix voltage increases by about 100 volts in going from 6,000 down to 4,500 mc because of slight dispersion in the phase velocity of the helix.

### 4.3 Operation Over an Extended Range

We now turn to a consideration of typical M1789 characteristics over an extended range of beam current, frequency, and magnetic field.* We shall concentrate on two items, the low-level gain and the maximum power output. From variations in these quantities the complete compression curves can be roughly deduced. This situation is illustrated in Fig. 27 which shows output as a function of input at different beam currents. While the shapes of these curves are slightly different, for the most part they can be derived from the 40-ma curve by shifting it along the abcissa

---

* The characteristics of the tube used for the low-level gain measurements in this Section were slightly different from those of the tube used for the maximum output measurements and both were slightly different from those of the tube used for the measurements of Section 4.2. All tubes, however, had characteristics falling within the ranges listed above.

by the amount the low-level gain changes, and along the ordinate by the amount the maximum output changes as beam current is varied. A similar procedure can be followed for variations with frequency and magnetic field. In all figures in this Section, parameters not being purposely varied were held at the nominal values given on page 1315.

*Low-level Gain*

Fig. 28 shows the variation in low-level gain with beam current and Fig. 29 shows its variation with helix voltage for several different beam currents. Fig. 30 shows the variation with frequency and Fig. 31 the variation with magnetic field.
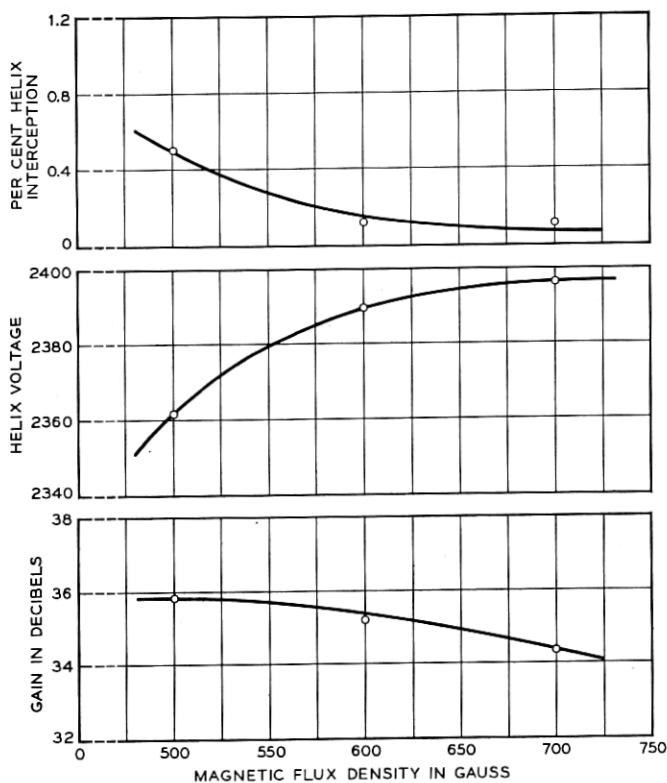


Fig. 31 — Low-level gain, helix voltage for maximum gain and helix interception at low signal level as functions of magnetic flux density. These measurements were made using different strength permanent magnet circuits. The gain varies with magnetic flux density mainly as a result of its effect on beam size and therefore on the degree of coupling between electron stream and helix. The helix voltage varies because of the effect of beam size on QC and therefore on the ratio of the optimum gain voltage to the helix synchronous voltage.
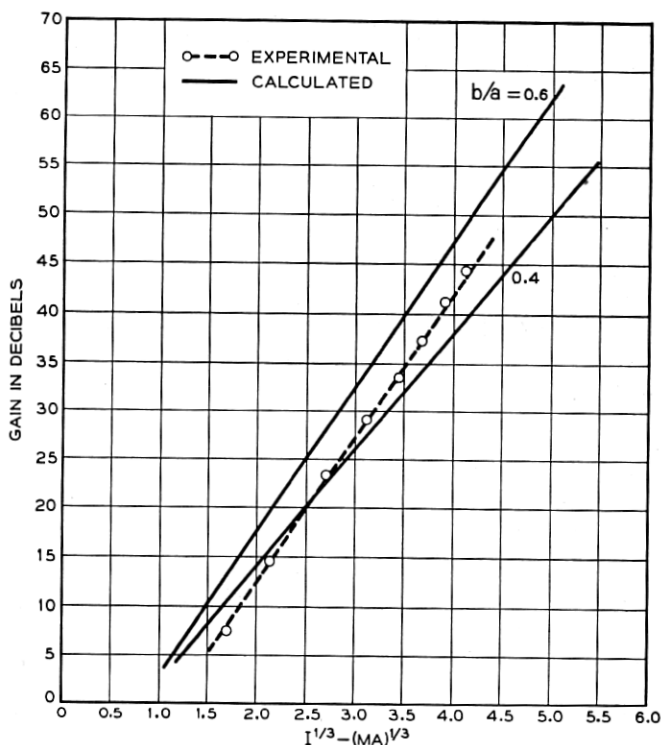
Fig. 32 — Measured and calculated low-level gain as a function of the one-third power of beam current. The parameter b/a is the ratio of effective beam diameter to mean helix diameter.
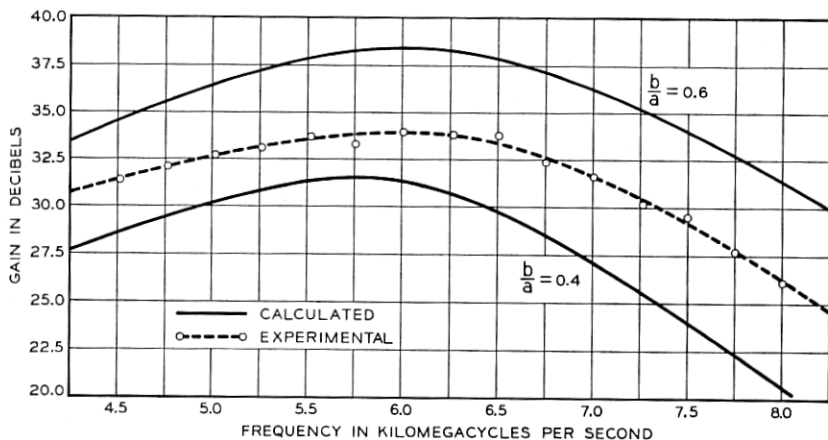


Fig. 33 — Measured and calculated frequency response for a current of 40 ma.

The observed gain compares well with that calculated from low-level TWT theory provided that we properly consider the effect of the helix attenuator and provided that we assume a $b/a$ of one-half. The method we have used in calculating the M1789 gain is discussed further in Appendix I. Fig. 32 compares the measured and calculated gain as a function of beam current and Fig. 33 compares them as a function of frequency. Fig. 34 shows measured and calculated ratios of voltage for maximum gain to synchronous voltage as a function of beam current. In all these figures calculations are shown for several values of the ratio of effective beam diameter to mean helix diameter $(b/a)$. We see that the effective value of $b/a$ appears to be about one-half. On the basis of measurements made by probing the beam of a scaled up version of a
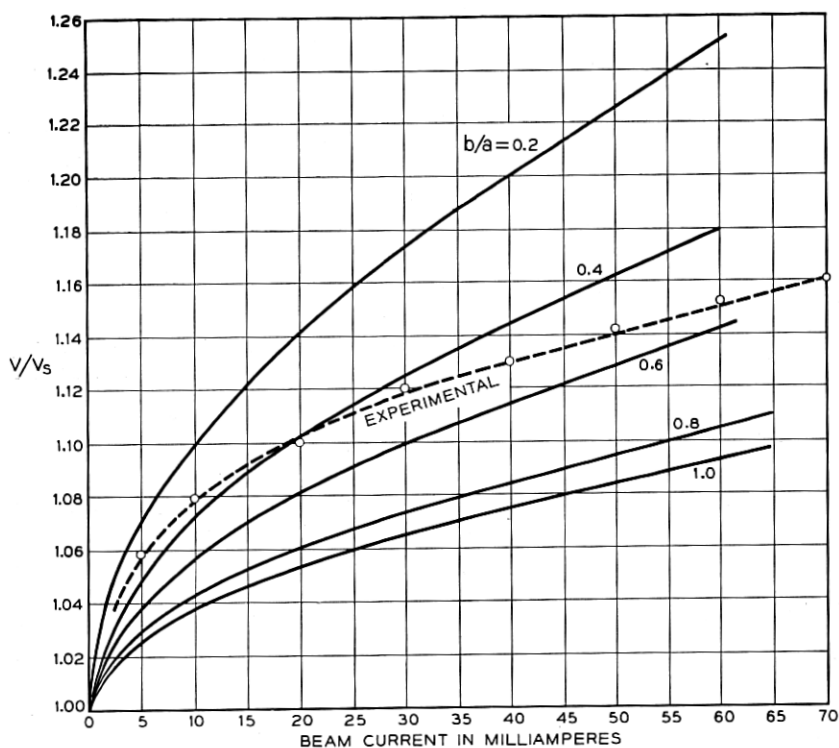


Fig. 34 — Measured and calculated ratio of voltage for maximum gain to synchronous voltage as a function of beam current. The calculated curves are shown for several values of the ratio of effective beam radius to mean helix radius (b/a). The location of the measured curve among the calculated ones is taken as an indication of the effective value of b/a in the M1789. At 40 ma it is about 0.5.
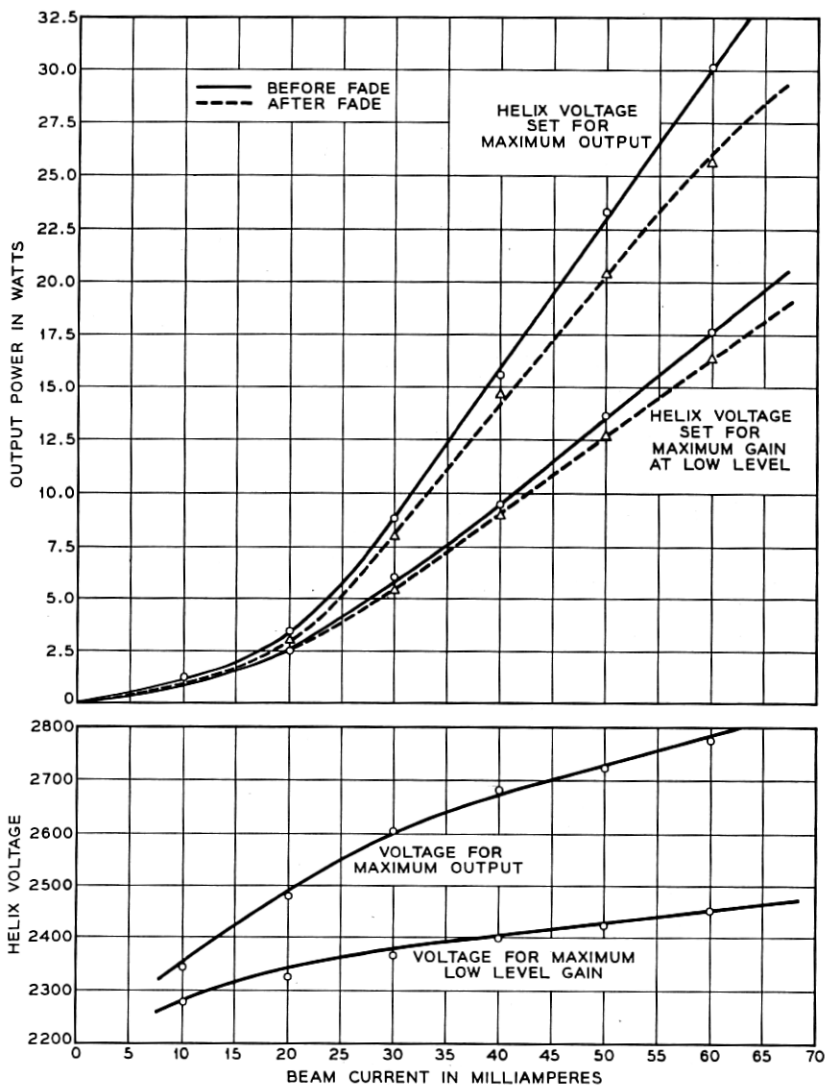
Fig. 35 — Maximum power output and helix voltage as functions of beam current. Curves are shown for before and after fading, and for the helix voltage adjusted for the maximum gain at low-level and for maximum output.
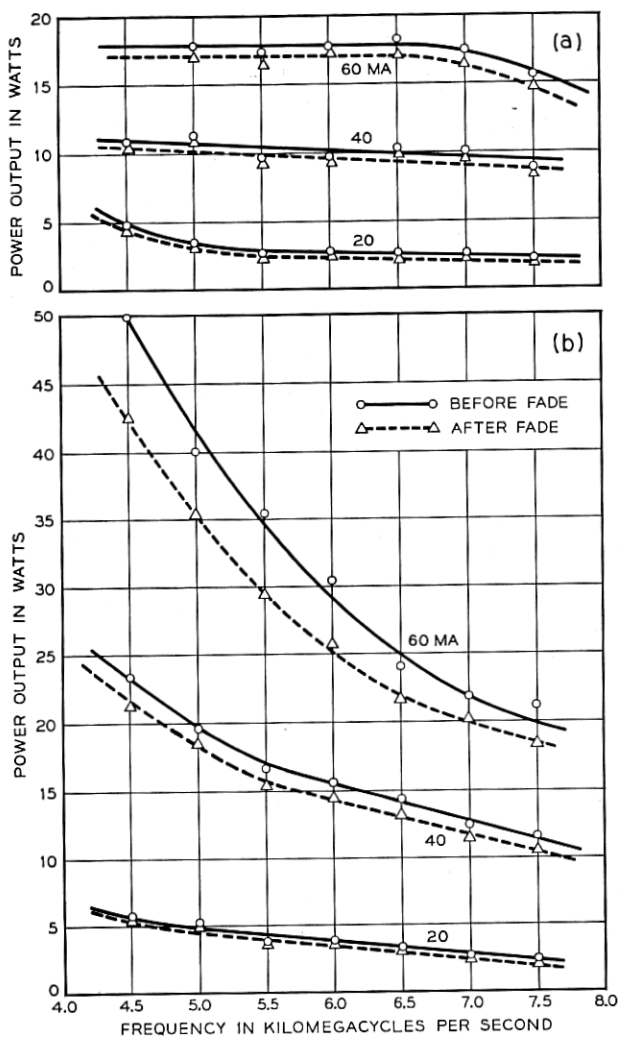
Fig. 36 — Maximum power output after fading as a function of frequency for several beam currents; in (a) with the helix voltage adjusted for maximum gain at low-level and in (b) with the helix voltage adjusted for maximum power output.
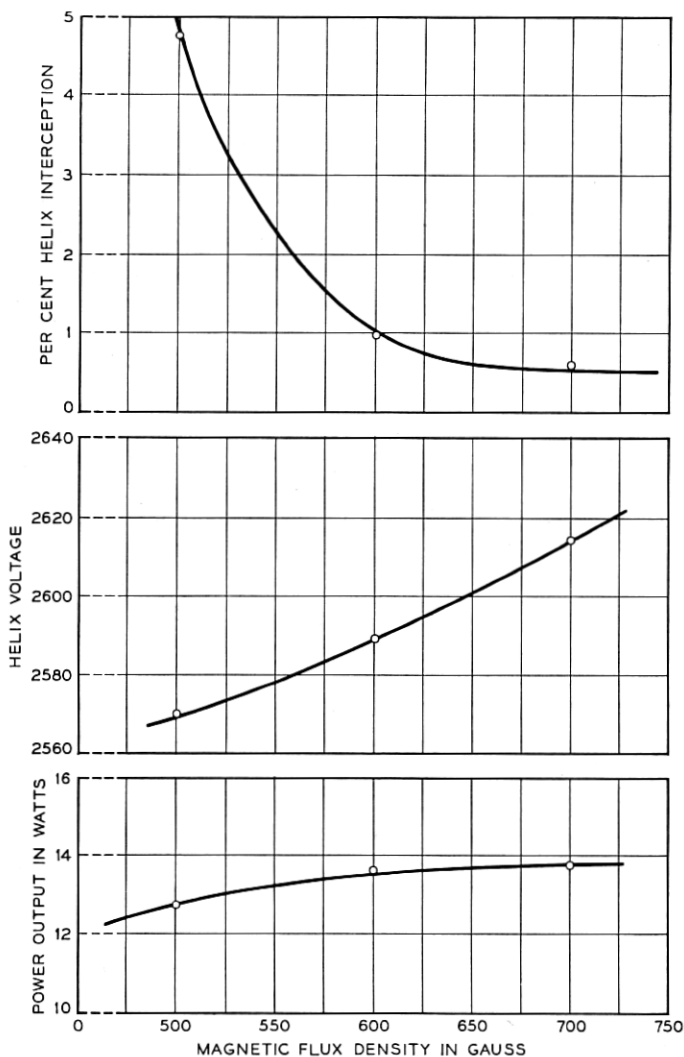
Fig. 37 — Maximum power output after fading, voltage for maximum output, and helix interception at maximum output as functions of magnetic flux density. These measurements were made using magnetic circuits charged to different strengths. Helix interception above about one per cent is undesirable if long tube life is required.

focusing system similar to that employed in the M1789, we estimate the actual beam diameter (for 99 per cent of the current) to be about 65 mils ($b/a = 0.7$). However, the current density distribution is peaked at the center of the beam because of the effect of thermal velocities of the electrons. Thus an effective $b/a$ of 0.5 is not unreasonable.

### Maximum Power Output

Fig. 35 shows the maximum power output as a function of beam current both immediately after rf drive is applied and after the tube has had time to stabilize. We see that at high rf power outputs the fading
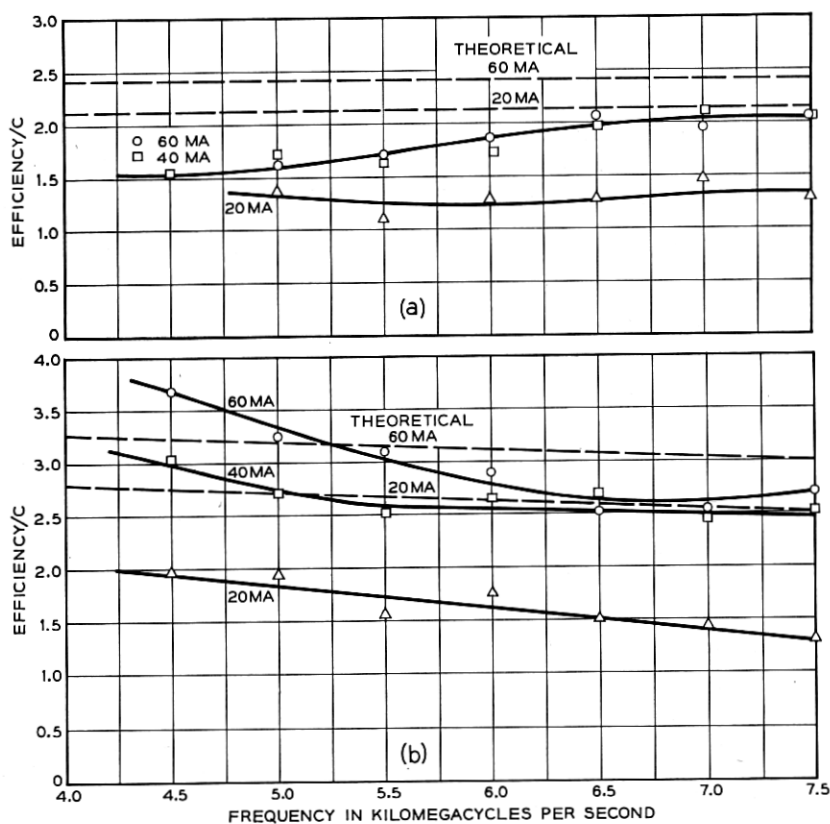


Fig. 38 — Ratio of electronic efficiency to gain parameter C as a function of frequency. The efficiencies used for this comparison are all before fading. The dotted lines are estimated from the Tien theory corrected for the intrinsic loss of the helix. The curves in (a) are for the case of the helix voltage adjusted for the maximum low-level gain and those in (b) for the case of the helix voltage adjusted for maximum power output.

becomes very serious and eventually limits the TWT output to about 30 watts. If it were necessary to reduce this fading, the envelope shrinking technique illustrated in Fig. 16 could be used. The maximum power output after fading is shown as a function of frequency for several beam currents in Fig. 36 and as a function of magnetic flux density in Fig. 37.

The theory of the high level behavior of a TWT[4] predicts that the ratio of electronic efficiency (i.e., $E$ = power output/beam power) to the gain parameter $C$ should be a function of $C$, $QC$ and $\gamma b$ (where $b$ is the beam diameter). However, with the range of parameters encountered in the M1789, the variation in $E/C$ should be small. Fig. 38(a) shows $E/C$ as a function of frequency when the TWT is operating at the voltage for maximum gain at low signal levels. Fig. 38(b) shows the maximum value of $E/C$ obtainable at elevated helix voltage. In both figures we show the efficiency as estimated using the results of Tien[4] corrected for the effect of intrinsic loss following the procedure of Cutler and Brangaccio.[5] All efficiencies in these two figures are the electronic efficiency before fading. It would be quite difficult to compare the efficiency after fading with theory because the intrinsic attenuation in this case varies along the helix in an unknown manner so that we cannot properly take it into account. From the figures we see that the calculated value of $E/C$ at 6,000 mc and 40 ma is not far from the experimental value but the experimental points show more variation with frequency than is predicted by theory. The low efficiency at 20 ma results from the fact that there is insufficient gain between the helix attenuator and the output. As a result, the TWT "overloads in the attenuation."

### 4.4 Noise Performance

A new and important noise phenomenon was observed in the course of the M1789 development. It was found that the noise figure is strongly dependent on the magnetic flux linking the cathode and on the rf output level of the TWT. For example, with the TWT operating near maximum output and with a cathode completely shielded from the magnetic field, noise figures of about 50 db were observed. By allowing 20 gauss at the cathode, the noise figure was reduced to 30 db. Fig. 39 shows the noise figure as a function of magnetic flux density at the cathode for several values of rf power output. We see that there is a peak of noise figure roughly symmetrical about zero flux at the cathode, and that the magnitude of this peak is considerably increased by operating the TWT at high output levels.

Some additional observed properties of the noise peak are:

(1) The magnitude depends on the synchronous voltage of the helix. For a 1,600-volt helix it is about 10 db higher than shown in Fig. 39 and

for a 2,600-volt helix it is about 5 db lower. The noise figure for 25 gauss at the cathode remains constant, however.

(2) There appears to be a threshold level of about 15-ma beam current below which the peak does not occur. Between 15 and 25 ma the peak increases. Above 25 ma it is roughly constant in magnitude.

(3) The peak can be considerably reduced by intercepting some of the edge electrons before they reach the helix region.

For this discussion it has been necessary to extend the concept of noise figure to the case of non-linear operation of the TWT. Essentially this noise figure is defined by the means we use to determine it. A block diagram of the equipment is shown in Fig. 40. The outputs of a calibrated broad band noise source and a signal oscillator are combined and used for the input to the TWT under test. The noise output from the TWT is passed through a filter tuned about 100 mc away from the signal so as to reject the carrier. It is then detected by a receiver tuned to the filter frequency. The noise figure is measured by turning the noise source off and on, noting the change in receiver output level and calculating the noise figure in the conventional manner. This procedure reduces to an ordinary noise figure measurement in the absence of input signal.

There are other ways that could be used to measure noise figure of a non-linear amplifier. A method more closely related to the use of the
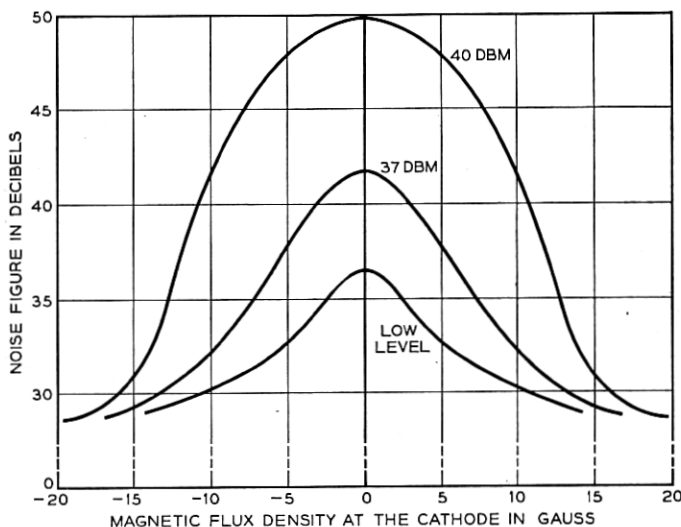


Fig. 39 — Noise figure as a function of magnetic flux density at the cathode for several values of rf power output. The flux density was varied by using an inductive heater through which ac current was passed. The present M1789 uses 19 gauss at the cathode, all of which is obtained from the focusing magnet — the heater now being non-inductive.

TWT in an FM radio relay was investigated briefly. In this measurement an FM receiver tuned to the carrier frequency was used to detect the noise modulation present in the TWT output. The noise figure was determined in the usual manner from the ratio of receiver outputs with the noise source turned off and on. When the TWT was operated in the linear region, this measurement gave the same result that our first method did. With the TWT operated in the non-linear region it gave a value within a few db of that obtained from the first method.

The cause of the high noise output observed for low magnetic flux densities at the cathode is at the present time not clearly understood. Fried at MIT and Ashkin and Rigrod at Bell Laboratories have all probed the beam formed by guns of the M1789 type and have found certain anomalous effects. Normally one would expect to find a standing wave of noise current along the electron beam. For the M1789 gun they find instead that after about two minima of the standing wave pattern, the noise current on the beam begins to grow and continues to do so until a saturation value is reached. The noise current at this saturation
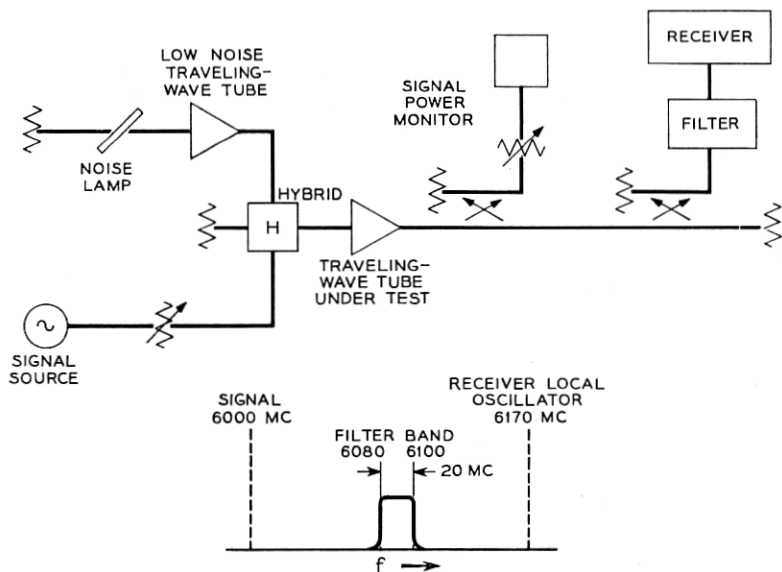


Fig. 40 — Block diagram of noise measuring equipment. The noise source consists of a fluorescent lamp the output of which is amplified by a low-noise TWT so as to bring the noise level to about 35 db above kTB at the M1789 input. The output from the M1789 is passed through a 20-mc bandpass filter which eliminates both the single frequency test signal and the noise in the image band of the receiver. The noise figure is measured by noting the difference in noise level at the receiver output with the noise source off and on, in a manner similar to that used in a conventional noise figure measurement.

value may be considerably higher than the original average noise level. As is the case with the noise figure in the M1789, the growing noise current has been found to be very sensitive to magnetic field at the cathode. By allowing sufficient field to link the cathode, the growing noise current can be eliminated leaving the normal noise current standing wave pattern on the beam. This phenomenon is not peculiar to the M1789 gun. It has been observed by various workers at MIT[6] and elsewhere on other guns producing beams with comparable current densities. A satisfactory explanation for it has not, at the time of this writing, been arrived at. It seems safe to say, however, that the growing noise current on the beam is the source of the high noise figures obtained in the M1789 when the cathode is completely shielded from the magnetic field.

### 4.5 *Intermodulation*

It has been found that certain intermodulation effects in the M1789 can be predicted from a knowledge of the compression and AM-to-PM conversion. Alternatively, these effects can be used to determine compression and AM-to-PM conversion. The procedure to be described has the advantage of being simple to implement as compared with the phase bridge arrangement of Fig. 24.
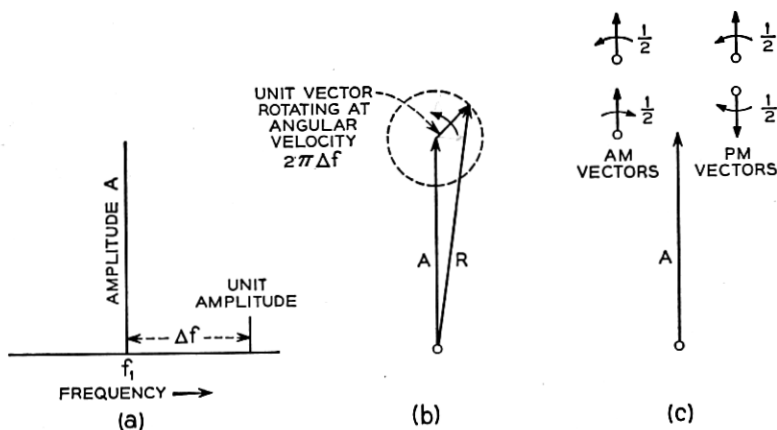


Fig. 41
(a) Spectrum of input signal to amplifier.
(b) Vector diagram of two input signals and the resultant signal (R) in a frame of reference rotating at an angular velocity $2\pi\Delta f$. Dotted line is the locus of the resultant signal.
(c) The rotating vector of the preceeding diagram can be broken down into a set of two vectors representing amplitude modulation and a set of two vectors representing frequency or phase modulation.

Intermodulation effects are ordinarily complicated and results are very hard to predict from single frequency measurements on an amplifier. For a TWT, however, one case — that in which two signals of very different amplitude are passed through the tube — can be treated simply. Consider an input to a TWT consisting of two signals at frequencies $f_1$ and $f_1 + \Delta f$ with the signal at $f_1$ being very much larger in amplitude. The composite signal applied to the amplifier will then be a signal at frequency $f_1$ which is amplitude and phase modulated at a rate $\Delta f$ in an amount proportional to the relative magnitudes of the two signals. This can be represented vectorially as shown in Fig. 41(a) and b. In this figure the amplitude of the signal $f_1 + \Delta f$ has been normalized to unity. "$A$" thus represents the ratio of the larger to the smaller signal. The locus of the resultant signal is shown by the dotted line. The single rotating vector can be considered as the sum of vectors at $f_1 + \Delta f$ and $f_1 - \Delta f$ as shown in Fig. 41(c). One set of vectors produces PM and the other AM. The AM and PM vectors cancel at $f_1 - \Delta f$ and add at $f_1 + \Delta f$.

Suppose this signal is put through an amplifier operating in compression. For the time being let us assume this amplifier has no AM-to-PM conversion. The compression in the amplifier will operate on the AM sidebands of the signal but will leave the PM sidebands unaffected. Let us define the quantity $c$ as a measure of compression in the amplifier by

$$c = 1 - \frac{\Delta V_0/V_0}{\Delta V_i/V_i} \tag{1}$$

where $V_0$ is the output voltage, $V_i$ input voltage, and $\Delta V_0$ is the change in output voltage for a change $\Delta V_i$ in the input voltage. This quantity is the per cent compression used in Section 4.2 divided by 100. If the signal in Fig. 41 is put through the amplifier while it is in compression, and the level of the signal at $f_1$ is subsequently brought back to amplitude $A$, we would then expect to have the situation shown in Fig. 42. Each AM sideband component has been multiplied by the factor $(1-c)$. The locus of the composite signal is now elliptical. Let $S_1$ and $S_2$ be the magnitude of the sidebands at $f_1 + \Delta f$ and $f_1 - \Delta f$ respectively. From Fig. 42 it is seen that

$$S_1 = \tfrac{1}{2} + \tfrac{1}{2}(1 - c) = 1 - c/2 \tag{2}$$

$$S_2 = \tfrac{1}{2} - \tfrac{1}{2}(1 - c) = c/2 \tag{3}$$

When $c = 0$, the amplifier is operating in the linear region and $S_1 = 1$,

$S_2 = 0$. This is the condition in Fig. 41. When the amplifier is operating as a perfect limiter, $c = 1$ and $S_1 = S_2 = 0.5$. Thus, in this case, the sideband $S_1$ is down 6 db from its value when the amplifier is operating i the linear region.

When there is conversion of AM-to-PM in the amplifier, the situation becomes somewhat more complex. Suppose an AM signal is fed into the amplifier and that its voltage is given by

$$V = V_1(1 + \alpha \sin \omega_m t) \sin \omega_c t \tag{4}$$

where $\omega_c$ and $\omega_m$ are the carrier and modulating radian frequencies and $V_1$ and $\alpha$ are constants. The outputs will be given by

$$V = KV_1[1 + \alpha(1 - c) \sin \omega_m t] \sin (\omega_c t + k_p \alpha \sin \omega_m t) \tag{5}$$

Here $K$ is the amplification, $c$ is the compression factor and $k_p$ is a factor which is a measure of the AM-to-PM conversion. It is seen that $k_p$ is the output phase change for a given fractional input change $\alpha$. Thus

$$k_p = \frac{\Delta\theta}{\alpha} \tag{6}$$

where $\Delta\theta$ is the phase change in radians caused by a fractional input change $\alpha$. Later on it will be desired to express $k_p$ in terms of degrees phase shift per db change in input amplitude. To express $\alpha$ in db we
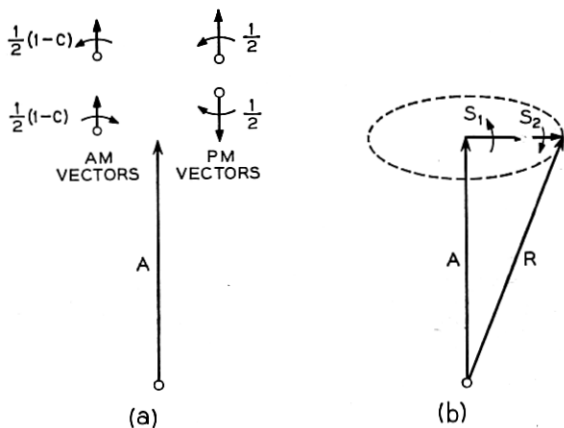


Fig. 42
(a) After passing through an amplifier in compression the AM sidebands are reduced in amplitude but the PM sidebands are unaffected. The lower two sidebands which represent a signal at frequency $f_1 - \Delta f$ no longer cancel and so there is a net signal at that frequency.
(b) The locus of the resultant signal now assumes an elliptical shape.

must evaluate $20 \log_{10} (1 + \alpha)$. The quantity $\log_e (1 + \alpha)$ can be ex-
panded in a series to give

$$\log_e (1 + \alpha) = \alpha - \frac{1}{2}\alpha^2 + \frac{1}{3}\alpha^3 + \cdots.$$

As long as $\alpha \ll 1$, we can approximate it by taking only the first term of
the above expression. Converting to the base ten and converting $\Delta\theta$
from radians as it appears in (6) to degrees, we find that

$$k_p = 0.152 \frac{\Delta\theta \text{ (in degrees)}}{\Delta \text{ input level (in db)}} \tag{7}$$

Now let us consider the case in which the signal of Fig. 41 is put
through an amplifier having AM-to-PM conversion. Fig. 43 shows the
vector picture of the resulting signal after the level of the signal at $f_1$
has been brought back to amplitude $A$. In this case the original PM
sidebands and the compressed AM sidebands are the same as in Fig. 42,
but there is now an additional set of PM sidebands as a result of the AM-
to-PM conversion. Since the peak deviation of output phase due to this
latter set of sidebands comes when the instantaneous amplitude is either
a maximum or a minimum, they are 90 degrees out of phase with the
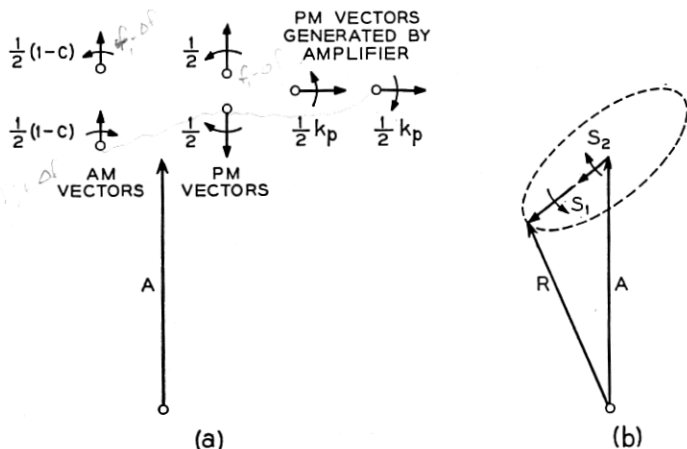other two sets of sidebands. From Fig. 43 it is seen that we can write



Fig. 43
(a) After passing through an amplifier having both compression and amplitude
to phase conversion, the AM vectors are reduced in magnitude and a new set of
PM vectors have appeared.
(b) The locus of the resultant signal of the vectors shown above is elliptical but
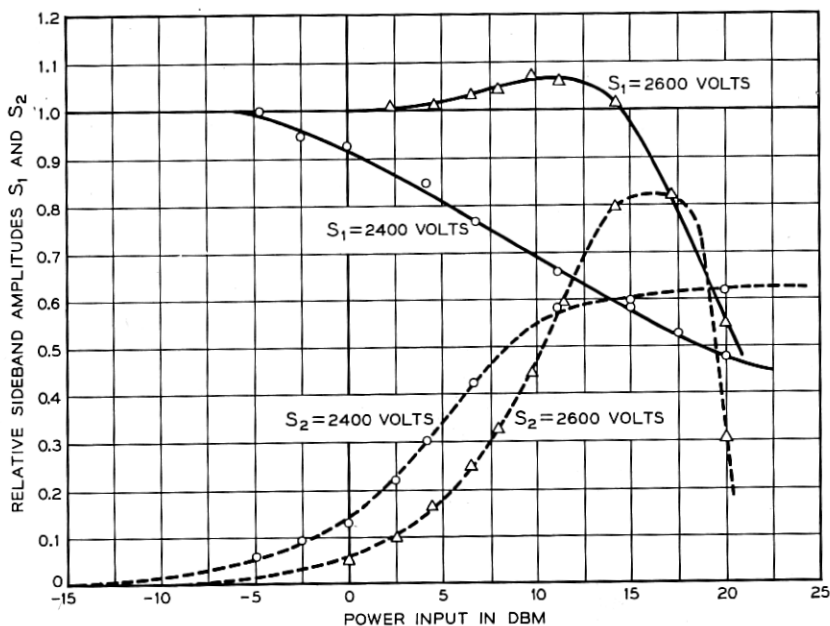the axis is tilted with respect to vector $A$.

Fig. 44 — Relative side band amplitudes $S_1$ and $S_2$ for the M1789 as a function of power input for two values of helix voltage.

for the sideband amplitudes $S_1$ and $S_2$ at $f_1 + \Delta f$ and $f_1 - \Delta f$ respectively

$$S_1^2 = [\tfrac{1}{2} + \tfrac{1}{2}(1 - c)]^2 + \left[\frac{k_p}{2}\right]^2 = (1 - c/2)^2 + \left(\frac{k_p}{2}\right)^2 \qquad (8)$$

$$S_2^2 = [\tfrac{1}{2} - \tfrac{1}{2}(1 - c)]^2 + \left[\frac{k_p}{2}\right]^2 = (c/2)^2 + \left(\frac{k_p}{2}\right)^2 \qquad (9)$$

Solving for $c$ and $k_p$ we obtain

$$c = 1 - (S_1^2 - S_2^2) \qquad (10)$$

$$k_p = 2\left[S_1^2 - \left(\frac{1 + S_1^2 - S_2^2}{2}\right)^2\right]^{1/2} \qquad (11)$$

Thus we see that from a measurement of the amplitudes $S_1$ and $S_2$ the values of $c$ and $k_p$ can be determined.

To check the validity of this approach to intermodulation, we determined the values of compression and AM-to-PM conversion for an M1789 from an intermodulation measurement and compared them with values obtained using the phase bridge set-up described in Section 4.2. In the intermodulation measurement the two signals were 100 mc apart
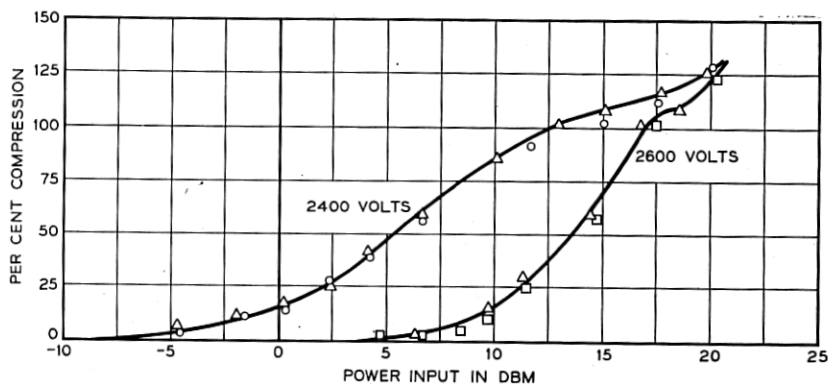
Fig. 45 — Compression as a function of input level for two values of helix voltage. Triangles represent data obtained with the test set of Fig. 24. Circles and squares represent data obtained by the two signal intermodulation measurement.

in frequency and 30 db different in level. From measurements of signal strength at the various frequencies involved, the magnitudes of $S_1$ and $S_2$ were determined with the results shown in Fig. 44. From these results the values of $c$ and $k_p$ were calculated and then converted to % compression and degrees per db in order to compare with the results of
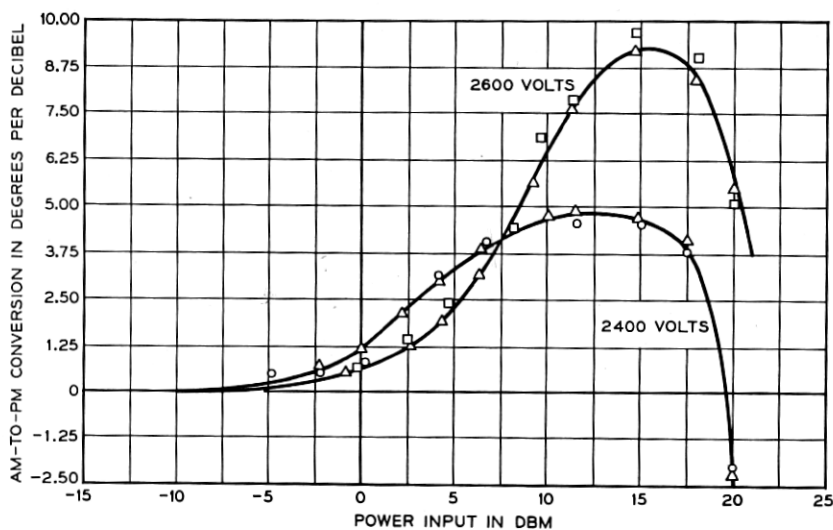


Fig. 46 — Conversion of amplitude modulation to phase modulation as a function of input level for two values of helix voltage. Triangles represent data obtained with the test set of Fig. 24. Circles and squares represent data obtained by the two signal intermodulation measurement.
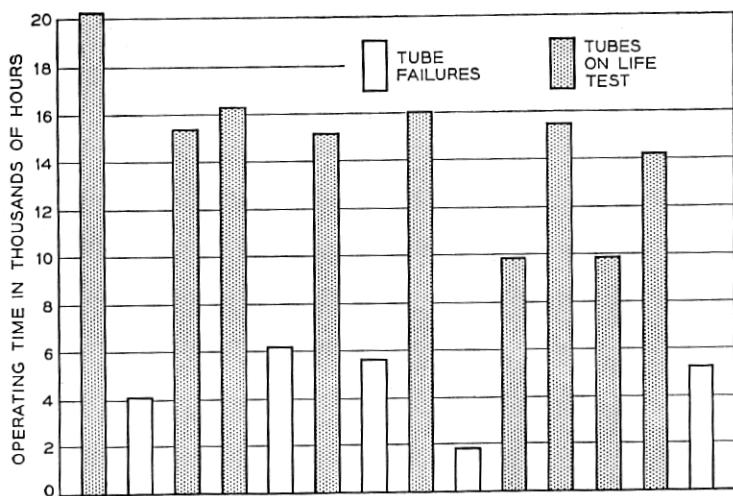
Fig. 47 — Life test results. The open bars indicate tubes that have failed; the solid bars tubes that were operating as of May 1, 1956. These tubes were operated with cathode temperatures between 720° and 760°C.

Figs. 23(c) and 23(e). The latter curves are repeated as Figs. 45 and 46 with the experimental points calculated from $S_1$ and $S_2$ shown. It is seen that the results of the two types of measurements compare remarkably well considering that the calculations of $c$ and $k_p$ both require the subtraction of nearly equal quantities. Thus we may conclude that our method of considering the intermodulation is substantially correct and that we can obtain compression and AM-to-PM conversion from an intermodulation measurement.

## V. LIFE TESTS

We feel that sufficient data have been accumulated to indicate that tube life in excess of 10,000 hours can be expected. Fig. 47 summarizes our life test experience. All tube failures were caused by cathode failure and these were evidently the result of exhaustion of coating. End of life for these tubes comes comparatively suddenly i.e., in a few hundred hours after the cathode current begins to drop. At this time the emission becomes non-uniform over the cathode surface with consequent beam defocusing and helix interception. This in turn causes gas to be released into the tube which then accelerates the cathode failure through cathode poisoning. The rf performance remained good over the tube life — the gain and output power actually increasing slightly near the end of life as the beam started to defocus.

## VI. ACKNOWLEDGMENTS

## APPENDIX I — GAIN CALCULATIONS

The gain calculations for the M1789 follow the procedure outlined by Pierce[7] with some minor modifications. The steps involved in the gain calculations for the loss free region of the helix are as follows:

(1) The experimental synchronous voltage is used to determine $\gamma a$ and the dielectric loading factor as defined by Tien.[8]

(2) From $\gamma a$ the value of helix impedance $K$ is obtained from Appendix VI of Pierce.[7]

(3) The value of $K$ is corrected using Tien's[8] results and $C$ is then calculated in the usual manner.

(4) The number of wavelengths $N_1$ per inch of helix is obtained using the experimentally determined (from synchronous voltage) wavelength.

(5) The value of $\omega_q/\omega$ is determined. In this calculation the curves for $\omega_p/\omega_q$ from Watkins[9] are employed.

(6) $QC$ is determined from

$$QC = \left(\frac{1}{2C}\frac{\omega_q}{\omega}\right)^2$$

(7) From $QC$, $B$ is determined from Fig. 8.10 of Pierce[7] and the gain $BCN_1$ in the loss free region is calculated.

In calculating the effect of the attenuator section, we have had to make some rather gross assumptions. Fortunately, it turns out that the

gain in the attenuator is a small fraction of the total gain in the tube so that the over-all gain is not particularly sensitive to the means we use for treating the attenuator. Essentially what we have done is to consider the high loss part of the attenuator as a severed helix region and the low loss part of the attenuator as a lossy helix region.

Fig. 48 shows the value of the growing wave parameter as a function of the loss parameter $d$ for various values of $QC$ as calculated from theory. Because of discontinuity losses to the growing wave as it propagates in a region of gradually increasing loss, the actual gain will be less than that calculated from Fig. 48. Some rather crude probe measurements have indicated that the effective $x$ vs. $d$ curve can be approximated by a straight line through the $d = 0$ and $d = 1$ points — the dotted line in Fig. 48.

Since the helix is effectively severed by the high loss portion of the attenuator we must subtract some discontinuity loss from the gain in the attenuator region. The effective drift length in the severed region is unknown so this discontinuity loss cannot be accurately calculated from the low-level theory. The discussion in chapter nine of Pierce[7] indicates that an average value of about 6 db is reasonable.

An alternate method of treating the attenuator was also tried. In this calculation, the $x$ vs. $d$ curves in Fig. 48 were assumed to be correct to
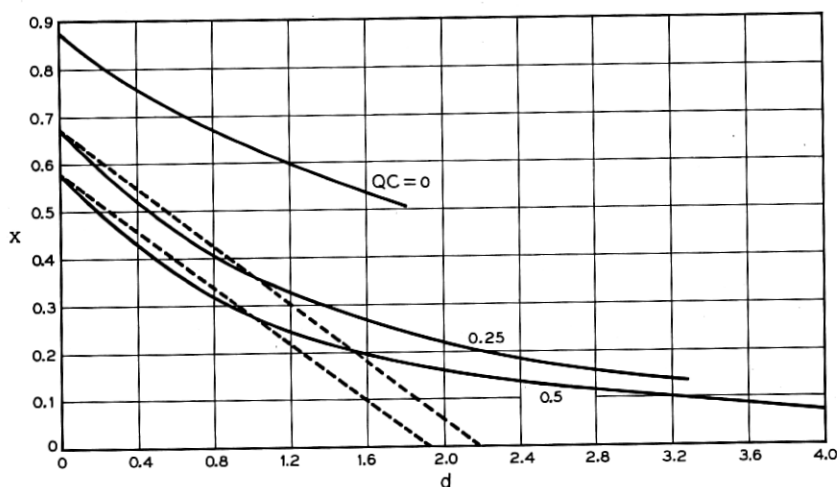


Fig. 48 — Curves of growing wave parameter x as a function of loss parameter d showing approximation (dotted lines) used in gain calculations for the M1789.

$d = 1$. The region for which $d > 1$ was considered as a severed helix region with 6-db discontinuity loss. Calculations using this procedure gave total gains for the TWT within a couple of db of the first method.

The remaining steps in calculating the gain of the TWT are therefore:

(8) The quantity $\alpha$ is determined from the slope of the dotted lines in Fig. 48.

(9) The length of helix, $\ell_e$ in the attenuator for which $x > 0$ is determined by using Fig. 48.

(10) The total attenuation $L$, in the section of the attenuator effective in producing gain is calculated.

(11) The initial loss parameter $A$ is obtained from Fig. 94 of Pierce.[7]

(12) The gain is calculated from

$$\text{Gain} = A - 6\text{db} + \alpha L + BCN_1 (3.5 + \ell_e)$$

where the six db is the discontinuity loss in the attenuator section and the 3.5 inches is the length of loss free helix.

GLOSSARY OF SYMBOLS

$\alpha$    loss factor from Pierce[7]

$A$    discontinuity loss parameter at input of helix from Pierce[7]

$B$    magnetic flux density or the space charge parameter from Pierce[7]

$B_B$    Brillouin flux density for a beam entirely filling the helix

$C$    gain parameter from Pierce[7]

$a$    helix radius

$b$    beam radius

$d$    loss parameter from Pierce[7]

$f$    frequency

$I_k$    cathode current

$I_a$    accelerator current

$I_h$    helix current

$I_c$    collector current

$k$    $2\pi/\lambda_0$ where $\lambda_0$ is the free space wavelength

$\ell_e$    length of helix attenuator in which gain is possible

$L$    loss in the part of the attenuator section which is capable of producing gain.

$N$    number of wavelengths in $TWT$

$N_1$    number of wavelengths on the helix per inch

$QC$    space charge parameter from Pierce[7]

$r_a$    anode radius of curvature of gun

$r_c$    cathode radius of curvature of gun

$r_{min}$    minimum beam radius from Pierce[10]

$r_c$   cathode radius

$r_{95}$   radius at the beam minimum through which 95 per cent of the current flows

$\sigma$   standard deviation of electron trajectory

$T_k$   cathode temperature

$V_a$   accelerator voltage

$V_h$   helix voltage

$V_c$   collector voltage

$x$   growing wave parameter from Pierce

$\omega$   radian frequency

$\omega_c$   carrier radian frequency

$\omega_m$   modulating signal radian frequency

$\omega_p$   radian plasma frequency

$\omega_q$   corrected radian plasma frequency

$c$   compression factor

$k_p$   AM-to-PM conversion factor

$\gamma$   radial propagation constant

## REFERENCES

1. Cutler, C. C., Spurious Modulation of Electron Beams, Proc. I.R.E., **44**, pp. 61–64, Jan., 1956.
2. Danielson, W. E., Rosenfeld, J. L., and Saloom, J. A., A Detailed Analysis of Beam Formation with Electron Guns of the Pierce Type, B.S.T.J. **35**, pp. 375–420, March, 1956.
3. Augustine, C. F., and Slocum, A., 6KMC Phase Measurement System For Traveling-Wave Tubes, I.R.E. Trans. **PGI-4**, Oct., 1955.
4. Tien, P. K., A Large Signal Theory of Traveling-Wave Amplifiers, B.S.T.J., **35**, pp. 349–374, March, 1956.
5. Brangaccio, D. J., and Cutler, C. C., Factors Affecting Traveling-Wave Tube Power Capacity, I.R.E. Trans. **PGED-3**, June, 1953.
6. Smullin, L. D., and Fried, C., Microwave Noise Measurements on Electron Beams, I.R.E. Trans., **PGED-4**, Dec., 1954.
7. Pierce, J. R., Traveling-Wave Tubes, D. Van Nostrand, Inc., 1950.
8. Tien, P. K., Traveling-Wave Tube Helix Impedance, Proc. I.R.E., **41**, pp. 1617–1623, Nov., 1953.
9. Watkins, D. A., Traveling-Wave Tube Noise Figure, Proc. I.R.E., **40**, pp. 65–70, Jan., 1952.
10. Pierce, J. R., Theory and Design of Electron Beams, D. Van Nostrand, Inc., 1949.